KU LEUVEN

FACULTY OF PHARMACEUTICAL SCIENCES

MASTER OF DRUG DEVELOPMENT

The interaction between LEDGF and MeCP2

The role in LINE-1 retrotransposition

THESIS

submitted by

Lena KWASPEN

Laboratory of Molecular Virology and Gene Therapy

Academic promotor: Prof. Dr. Zeger DEBYSER

Supervisor: Laura DEBUSSCHERE

LEUVEN

Academic year 2022-2023

Dankbetuiging

Na het schrijven van mijn masterthesis zou ik graag met enige fierheid enkele personen willen bedanken die deze masterthesis mede mogelijk hebben gemaakt.

Als eerste zou ik graag professor Zeger Debyser willen bedanken voor het uitbouwen van zijn onderzoeksgroep en mij de kans te geven er mijn stage te volbrengen. Bedankt voor uw duwtjes in de rug en de richting die u me gegeven heeft tijdens de mini-meetings. Daarbij aansluitend zou ik graag mijn stage-begeleidster, Laura Debusschere, willen bedanken om mij dit jaar te begeleiden. Het was een intensief jaar. Bedankt voor je geduld, raad en het meermaals nalezen van mijn masterthesis. Ook bedankt aan Saskia Lesire, om me te begeleiden bij het *in vitro* project. Ik vond het zeer uitdagend om mijn experimenten tot een goed einde te brengen. Graag wil ik heel MolMed bedanken. Bedankt om op al mijn vragen te beantwoorden, om tijd voor me vrij te maken als ik aan de deur kwam kloppen. Bedankt voor de interesse in mijn project en de schouderklopjes na een geslaagde mini-meeting of mid-term presentatie.

Dankjewel aan mijn Jericho kotgenoten! Bedankt om ‘s morgens met me koffie te drinken, voor de knuffels, de deugddoende kotmaaltijden en de gezellige babbels tot diep in de nacht. Maar vooral bedankt voor de warme plek waar ik altijd thuis mag komen. Ik heb me dit jaar echt gedragen gevoeld.

Dit jaar was gevuld met vele ingrediënten om deze masterthesis mogelijk te maken. Maar het snufje zout dat voor mij dit jaar net een beetje meer pit heeft gegeven was het Translational Medicine programma georganiseerd door I^{3}H. Tijdens deze modules heb ik de nood aan diversiteit, communicatie en samenwerking mogen ervaren op een heel persoonlijke manier. Deze ervaring was inspirerend en persoonsvormend voor me. Ik zal niet stoppen met vragen stellen en interpersoonlijke connecties te leggen.

Als laatste zou ik graag mama en papa willen bedanken voor de trots blik, de bemoedigende glimlach en het onuitputtelijk vertrouwen in mij. Bedankt voor het lekkere eten, de koffietjes, de interesse in mijn onderzoek en het vele enthousiasme! Afsluiten zou ik graag met mijn kat, Poes, te bedanken. Ze was mijn studiemaatje doorheen mijn universitaire studies. Ik hoopte dat ze dit moment nog meemaken mocht.

TABLE OF CONTENT

LIST OF ABBREVIATIONS

aa	Amino acid
AAV	Adeno-associated virus-based
ATH	AT-hook motives
C	Cysteine-rich domain
cDNA	Complementary DNA
CpG	Cytosine-guanine
CR	Charged regions
CTD	C-terminal domain
CTT	Carboxy-terminal tail
DMEM	Dulbecco's modified Eagle's medium
EGFP	Enhanced green fluorescent protein
EN	Endonuclease
FOXA1	Forkhead box protein A1
GAPDH	Glyceraldehyde 3-phosphate dehydrogenase
GC/mL	Genome copies/mL
H3K27me3	Histone 3 is 3 times methylated on lysine 27
H3K36me2	Histone 3 is 2 times methylated on lysine 36
H3K36me3	Histone 3 is 3 times methylated on lysine 36
HEK	Human embryonic kidney
HIV	Human immunodeficiency virus
IBD	Integrase binding domain
ID	Intervening domain
KAP1	KRAB-associated protein 1

KO	Knock-out
LEDGF	Lens epithelium-derived growth factor
LINE-1	Long interspersed element 1
LTM	Long-term memory
LTRs	Long terminal repeats
MBD	Methyl binding domain
MDS	MeCP2 duplication syndrome
MeCP2	Methyl CpG binding protein 2
NID	NCoR interaction domain
NLS	Nuclear localization signal
Non-LTRs	Non-long terminal repeats
NTD	N-terminal domain
ORF	Open reading frame
PCR	Polymerase chain reaction
PML-NBs	Promyelocytic leukaemia protein-nuclear bodies
PSIP1	PC4- and SFRS1- interacting protein 1
PWWP	proline-tryptophan-tryptophan-proline
qPCR	Quantitative polymerase chain reaction
RB1	Retinoblastoma protein
RNAP 2	RNA polymerase 2
RNP	Ribonucleoprotein
ROI	Region of interest
RT	Reverse transcriptase
RT-qPCR	Reverse transcription-quantitative polymerase chain reaction
RTT	Rett syndrome

SD	Standard deviation
sgRNA	Single guide RNA
SINE	Short interspersed element
SIRT6	Sirtuin 6
SN	Substantia nigra
TE	Transposable elements
TH	Tyrosine hydroxylase
TPRT	Target-primed reverse transcription
TRD	Transcription repression domain
TREX1	Three-prime repair exonuclease 1
UTR	Untranslated region
VLP	Virus-like particle
VTA	Ventral tegmental area
WT	Wild type
XCI	X-chromosome inactivation

Summary

Methyl CpG binding protein 2 (MeCP2) is a key driver of Rett syndrome, while lens epithelium-derived growth factor (LEDGF) is a molecular tether of the human immunodeficiency virus (HIV) integrase towards the human genome, and both proteins interact with each other. Moreover, MeCP2 binds to single methylated cytosine-guanine sites in the long interspersed element 1 (LINE-1) promoter. LINE-1 is a transposable element, which moves through the genome via a "copy and paste" mechanism. This process is mainly known as retrotransposition. LINE-1 retrotransposition is correlated with several diseases such as cancer, metabolic disorders, neurological disorders, genetic disorders and autoimmune diseases. However, the activation of the LINE-1 retrotransposition process is not fully understood. Therefore, more research is needed to unravel the role of the MeCP2-LEDGF interaction during LINE-1 retrotransposition.

In this master's thesis a knock-out (KO) cell line of the *MeCP2 gene* and a KO cell line of the *PC4- and SFRS1- interacting protein 1 (PSIP1)* gene are created with murine leukemia virus-based virus like particles (VLPs) and validated, in order to determine which genes are regulated by the MeCP2-LEDGF protein complex. The transfection experiment resulted in the selection of MeCP2-construct 1 and LEDGF-construct 2 as the most promising constructs. The *PSIP1* KO cell line was successfully created and LEDGF proteins levels are reduced by 99%. The *MeCP2* KO cell line was less successful, even though MeCP2 proteins are reduced with 92%, residual proteins were still visible. Therefore, only the *PSIP1* KO cell line can be used in further experiments, in contrast to the *MeCP2* KO, which did not have a complete KO.

The interaction between LEDGF and MeCP2 in the mouse brain, was confirmed by Li et al. (1). This master's thesis studies the influence of a *PSIP1* KO on MeCP2 protein levels in different brain regions of *PSIP1*$^{fl/fl}$ mice. Regional injections with a CMViesynapsin-intron-Cre adeno-associated virus 2/7-based vector were performed to generate the local KO. The regional *PSIP1* KO mouse model was validated and the results confirm a locally induced *PSIP1* KO in the transduced regions. The observed reduction in LEDGF protein levels was not due to neurotoxicity. Furthermore, a KO of the *PSIP1* gene in the cortex, hippocampus and substantia nigra revealed a decrease in MeCP2 protein levels. The validated mouse model can be used in further research. The reported results support the hypothesis that LEDGF has an influence on MeCP2 in different brain regions.

Samenvatting

Methyl CpG binding protein 2 (MeCP2) is de drijver van het Rett syndroom, terwijl lens epithelium-derived growth factor (LEDGF) een moleculaire schakel is die het humaan immunodeficiëntie virus (HIV) integrase naar het menselijk genoom brengt en beide proteïnen interageren met elkaar. Bovendien bindt MeCP2 aan gemethyleerde cytosine-guanines in de long interspersed element 1 (LINE-1) promotor. LINE-1 is een overdraagbaar element dat door het genoom beweegt via een "kopieer en plak"-mechanisme. Dit proces is beter gekend als retrotranspositie. LINE-1 retrotranspositie is gecorreleerd aan verschillende ziektes zoals kanker, metabole aandoeningen, neurologische aandoeningen, genetische aandoeningen en auto-immuunziektes. Het activatieproces van LINE-1 retrotranspositie is desondanks nog niet volledig in kaart gebracht. Daarom is er meer onderzoek nodig naar de MeCP2-LEDGF interactie tijdens LINE-1 retrotranspositie.

In deze masterthesis wordt er een knock-out (KO) cellijn gemaakt via murine-leukemie-virus gebaseerde virusachtige partikels en gevalideerd voor het MeCP2 gen en voor het *PC4- and SFRS1- interacting protein 1 (PSIP1)* gen. Deze cellijnen hebben als doel om te kunnen bepalen welke genen gereguleerd zijn door het MeCP2-LEDGF proteïne-complex. Het transfectie-experiment resulteerde in de selectie van MeCP2-construct 1 en LEDGF-construct 2 als de meest belovende constructen. De *PSIP1* KO cellijn is succesvol gecreëerd en de LEDGF eiwitlevels zijn gereduceerd met 99%. De *MeCP2* KO cellijn was minder succesvol. Alhoewel de MeCP2 eiwitlevels gereduceerd zijn met 92%, waren nog steeds residuele eiwitten zichtbaar. Daarom kan enkel de *PSIP1* KO cellijn verder gebruikt worden in komende experimenten, in tegenstelling tot de *MeCP2* KO cellijn die geen volledige KO gaf.

De interactie tussen LEDGF en MeCP2 in de hersenen van de muis is bevestigd door Li et al. (1). Deze masterthesis bestudeert in *PSIP1*$^{fl/fl}$ muizen de invloed van een PSIP1 KO op MeCP2 eiwitlevels in verschillende hersenzones. Plaatselijke injecties met een CMViesynapsin-intron-Cre adeno-geassocieerde virus 2/7 gebaseerde vector zijn uitgevoerd om een lokale KO te creëren. Het plaatselijke *PSIP1* KO muismodel is gevalideerd en de resultaten bevestigen een lokaal geïnduceerde *PSIP1* KO in de getransduceerde regio's. De geobserveerde reductie in LEDGF eiwitlevels was niet vanwege neurotoxiciteit. Bovendien onthulde de KO van het *PSIP1* gen in de cortex, hippocampus en substantia nigra een daling in MeCP2 eiwitlevels. Het gevalideerde muismodel kan gebruikt worden in verder onderzoek. De gerapporteerde resultaten ondersteunen de hypothese dat LEDGF een invloed heeft op de MeCP2 eiwitlevels in verschillende hersenregio's.

1 INTRODUCTION

1.1 TRANSPOSABLE ELEMENTS

Transposable elements (TEs) were discovered by Barbara McClintock in the 1950s (2, 3). For a long period, TEs were considered "junk" DNA. Nowadays, the scientific vision towards DNA is a complicated structure that is constantly changing. TEs enable DNA to respond to environmental changes and contribute to the onset of diseases (3, 4). Therefore, the vision of TEs as “junk” DNA is outdated (3).

The human genome consists for 45% of TEs, of which some are still active (3). There are two main groups in the classification of TEs, DNA transposons and retrotransposons. The first group moves through the genome via a “cut and paste” mechanism, with a DNA intermediate (5, 6). These are called DNA transposons. DNA transposons are still active in bacteria, but are inactivated by mutations in higher organisms such as humans. About 3% of the human genome consists of these inactive molecular fossils (4, 6, 7, 8). The second group are retrotransposons. It is hypothesised that during the Eocene, 56 to 33.9 million years ago, ancient subfamilies of the retrotransposons found their way into the genome (8, 9). Throughout evolution, most of the retrotransposons got inactivated by mutations but the variants that are still active use an RNA intermediate to move through the genome using a “copy and paste” strategy. Retrotransposition occurs during embryonal development, neural stem cell differentiation to neurons and during lifespan. Different regions and rates of retrotransposition establish variation between individuals (4, 7, 8). The classification of TEs is shown in Figure 1.1.

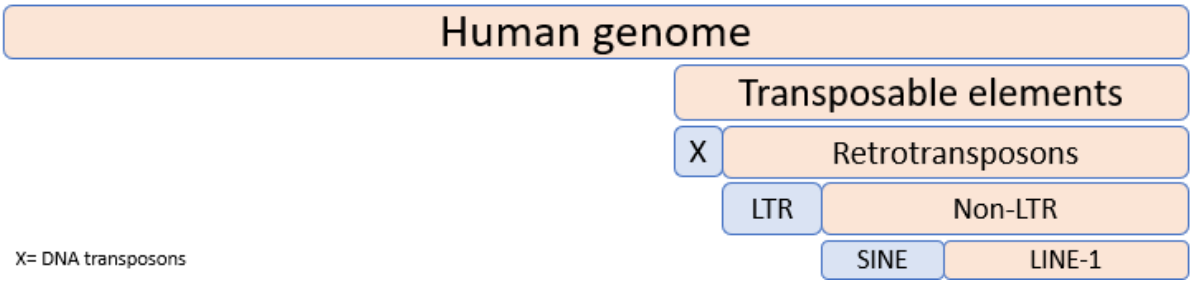

Figure 1.1: Classification of transposable elements. Transposable elements can be divided into two groups: DNA transposons and retrotransposons. Retrotransposons can be further divided into two subgroups: long terminal repeats (LTRs) and non-long terminal repeats (non-LTRs). Furthermore, non-LTRs consist of short interspersed elements (SINEs) and long interspersed element 1 (LINE-1). The orange colour indicates the classification to which LINE-1 belongs.

Retrotransposons are further divided into two subgroups: long terminal repeat (LTR) and non-long terminal repeat (non-LTR) retrotransposons (4, 7, 8). LTR retrotransposons make up 8% of the human genome. In literature, LTR retrotransposons are sometimes referred to as human endogenous retroviruses because of the virus-like sequences and the characteristic long repeats at each end (7, 10). LTR retrotransposons contain promoters, enhancers, transcription binding sites and polyadenylation signals (7, 10, 11, 12). LTR retrotransposons lost most of their retrotransposition activity and thereby

the ability to affect the genome by the occurrence of mutations (7, 10, 11). In contrast to previous TE, the group known as non-LTR retrotransposons, also referred to as poly-A retrotransposons, is the only one that undergoes active retrotransposition (7, 13). Short interspersed element (SINE) and long interspersed element 1 (LINE-1) are subgroups from the non-LTR retrotransposons that all end with a 3' poly-A tail (13). SINEs represent 10-13% of the human genome. These are non-autonomous elements, which means that their genome does not carry the sequence to encode enzymes necessary for mobilisation. Therefore, the retrotransposition of SINEs depends on LINE-1 element-derived proteins (7, 8).

1.1.1 Structure and function of LINE-1

The human genome consists for 17-21% of LINE-1 elements (4, 7, 8). This means that more than 500 000 LINE-1 sequences are present in the human genome. From all those sequences, only 0.02% of LINE-1 elements undergo active retrotransposition (7, 8). LINE-1 is a 6kb, active, autonomous, transposable element (4, 7, 8). A LINE-1 element consists of a 5' untranslated region (UTR) with an internal RNA polymerase 2 (RNAP 2) sense and antisense promoter, two open reading frames (ORF) 1 and 2, and a 3' UTR that terminates in a poly-A tract (6, 8). A 63-nucleotide spacer with two in-frame stop codons separates ORF1 and ORF2 from each other. The structure of a LINE-1 element is shown in Figure 1.2. LINE-1 encodes for three proteins: ORF1p, ORF2p and ORF0p (14). These proteins are important in LINE-1 retrotransposition (15).

LINE-1 elements differ between humans and mice. Unlike the human genome, 19% of the mouse genome consists of 3000 active LINE-1 elements (16). The mouse LINE-1 element is one 1kb larger than the 6kb human LINE-1 elements (16, 17). The 5' UTRs of a mouse LINE-1 element divide them into subfamilies. Subfamily A, Tf and Gf have been proven to undergo retrotransposition. Remarkably, human LINE-1 constructions have the ability to undergo retrotransposition in mice or mouse-derived cells and *vice versa* (16).

The ORF1p, is the protein encoded by the ORF1 of LINE-1 (18). ORF1p is a 40 kDa protein with a sequence-independent RNA-binding capacity, which is required for ribonucleoprotein (RNP) formation. The N-terminus of the ORF1p has a coiled-coil domain, which facilitates the trimerization of these proteins. The central part and the C-terminal domain of the ORF1p create the ability to bind to RNA. Furthermore, the ORF1p contains a nucleic acid chaperone activity that facilitates the re-annealing of single-stranded DNA *in vitro* (6, 8, 15, 19).

The ORF2p, is a 150 kDa protein with two enzymatic activities. The ORF2p has a N-terminal apurinic/apyrimidinic-like endonuclease activity (EN) followed by a reverse transcriptase (RT) activity (6, 8). ORF2p has also a cysteine-rich domain (C) at its C-terminus. However, the exact function of this

domain in the LINE-1 retrotransposition process is not known (6, 20). The non-sequence specific RNA binding capacity relies on the last 180 last amino acids (aa) of the ORF2p. The ORF2p is the essential part of a LINE-1 element for the non-autonomous retrotransposition of SINEs. Consequently, mutations in ORF1p or ORF2p prohibit retrotransposition (4, 6).

In 2015, Ahmet et al. discovered the sequence for the ORF0p in the antisense strand of the 5' UTR (14). The activity of the antisense promoter is one eight of the activity of the sense promotor and is dependent on the methylation state (21, 22). The ORF0p is a 71 aa protein derived of the antisense promoter (22). When ORF0p is overexpressed in human embryonic kidney (HEK) 293T cells and human embryonic stem cell-derived neural progenitor cells, an increased LINE-1 mobility is observed (8, 14). Furthermore, when the antisense promotor is activated, Honda et al. saw an increase in ORF0p and cell growth (21). Moreover, ORF0p has a role in cell division. ORF0p is localised in the nucleus close to promyelocytic leukaemia protein-nuclear bodies (PML-NBs). PML-NBs are tumour suppressor genes related to several cellular processes (21, 23). Activation of the antisense promotor promotes mitosis via ORF0 and PML-NBs pathways resulting in enhanced cell division (21).

The 3' UTR region in LINE-1 is 206kb long and has a polypurine tract. This tract is forming quadruplexes (6). Quadruplexes are coplanar arrangements of guanines and are held by Hoogsteen hydrogen bonds and stabilised by cations (24). However, Piskareva et al. discovered that 3' UTR quadruplexes suppress reverse transcription activity *in vitro* by inhibiting the target-primed reverse transcription (TPRT) (6, 8, 25). The quadruplexes, in the RNA template or in the growing DNA strand, form a barrier to TPRT. These complexes affect the expression of neighbouring genes as well. As people become older, the potential of gene-regulatory quadruplexes is decreasing due to mutations (24, 26). Therefore, it is supposed that quadruplexes regulate the speed of retrotransposition (26). Furthermore, the 3' UTR region has a poly-A tail, which is recognised by RNAP 2. These poly-A signals are relatively weak. RNAP 2 occasionally does not stop at the signal which results in the incorporation of genomic DNA in LINE-1 3' UTR (6, 24, 26).

1.1.2 The mechanism of retrotransposition

Retrotransposition starts at the LINE-1 5' sense promoter, which is an RNAP 2 promoter that initiates the transcription of the full-length *LINE-1* gene into LINE-1 mRNA. LINE-1 mRNA is transported into the cytoplasm and translated into ORF1p and ORF2p (4, 6). ORF1p and ORF2p bind to their mRNA and form an RNP, which is a crucial step in the retrotransposition process (27).

To create a RNP, three ORF1 proteins assemble together to form trimers. Several trimers bind to the LINE-1 mRNA to protect and mobilise this mRNA (18, 22, 27). Only one ORF2p binds to a mRNA to finally form a complete RNP (20, 28, 29). A single ORF2p is necessary for inserting a LINE-1 element

into the genome (28, 29). ORF2p is difficult to detect *in vitro* because the required amount of protein for retrotransposition is low (28).

During the formation of a RNP, ORF1p and ORF2p can adopt a *cis*- and a *trans*-conformation. The activity of the RNP depends on this conformation. The *trans*-conformation is necessary for the retrotransposition of non-autonomous SINE elements and pseudogenes (6, 7, 27, 30). Pseudogenes originate from cellular mRNA that undergoes TPRT (7). Altogether, 8000 to 17000 processed pseudogenes are present in the human genome (6). On the other hand, the *cis*-conformation favours the binding to LINE-1 mRNA (28).

When the mRNA is included in the RNP, translation stops because the mRNA is not available anymore to the ribosomes (22). An unidentified process returns the RNP back into the nucleus (4, 6, 7, 8). However, Taylor et al. suggested that ORF1p deliver the RNP to the nucleus during cell division (31). According to this theory, ORF1p does not enter the nucleus but is necessary for the nuclear entry of the only ORF2p containing RNP (31). However, the fact that ORF1p has nucleic acid chaperone activity which can play a role in the nucleic acid arrangements during TRPT is at odds with this theory (19).

When the RNP enters the nucleus it locates around the genome. TPRT starts with the EN-function of ORF2p that cleaves one of the double-stranded DNA strains of the target site into single-stranded DNA at a 3' ATTTT 5' motive. Nevertheless, the EN of ORF2p can also create a double-stranded break. As a conclusion, it is not fully clear what happens with the second strand during TPRT (6, 7, 8, 17, 32). The poly-A tail of the LINE-1 mRNA binds to the TTTT motive of the antisense strand and reverse transcription by ORF2p assures the transition of mRNA into DNA (6, 7). Figure 1.2 shows the retrotransposition cycle of LINE-1 (20). Truncation and additional inactivation occur when TPRT is not selective or not successful. For example, the mRNA may fold double and create an insertion. Alternatively, the EN of ORF2p in the RNP can still be active after mRNA binding to the DNA and cleave the genomic DNA which results in a deletion (6). Furthermore, DNA repair processes can result in a 5' truncation of the newly copied LINE-1 element (4).

1.1.3 Physiological function of LINE-1 in the brain

LINE-1 plays a physiological role in the brain during memory formation (33). The hippocampus is a brain region involved in memory formation and also a susceptible region for LINE-1 retrotransposition (34). LINE-1 retrotransposition has an important role in long-term memory (LTM) formation. LINE-1 expression and retrotransposition are increased in the hippocampus of mice upon training (33). In depleted LINE-1 retrotransposition mouse models, LTM formation is impaired. However, short-term memory does not show any alterations (33). It has been shown that voluntary exercise, in ten to twelve weeks old mice, leads to the proliferation of hippocampal progenitor cells. This proliferation

contributes to neurogenesis. Additionally, in the hippocampus of mice that do exercise, an increase in LINE-1 retrotransposition was observed. Taken all together, LINE-1 retrotransposition contributes to neuronal plasticity, which is a mechanism to adapt to environmental changes (4, 35). In contrast to the previous study, LTM is declined in Drosophila Argonaute 2 upon ageing. Drosophilas Argonaut 2 have elevated expression of TEs due to a mutation in silencing proteins of TE. The mutant flies display a decrease in LTM. The older mutant flies have an even stronger decrease in LTM compared with young mutant flies. These results suggest that age plays an additional role in the LTM formation (36). Further research has to be done if the results can be translated to other species.

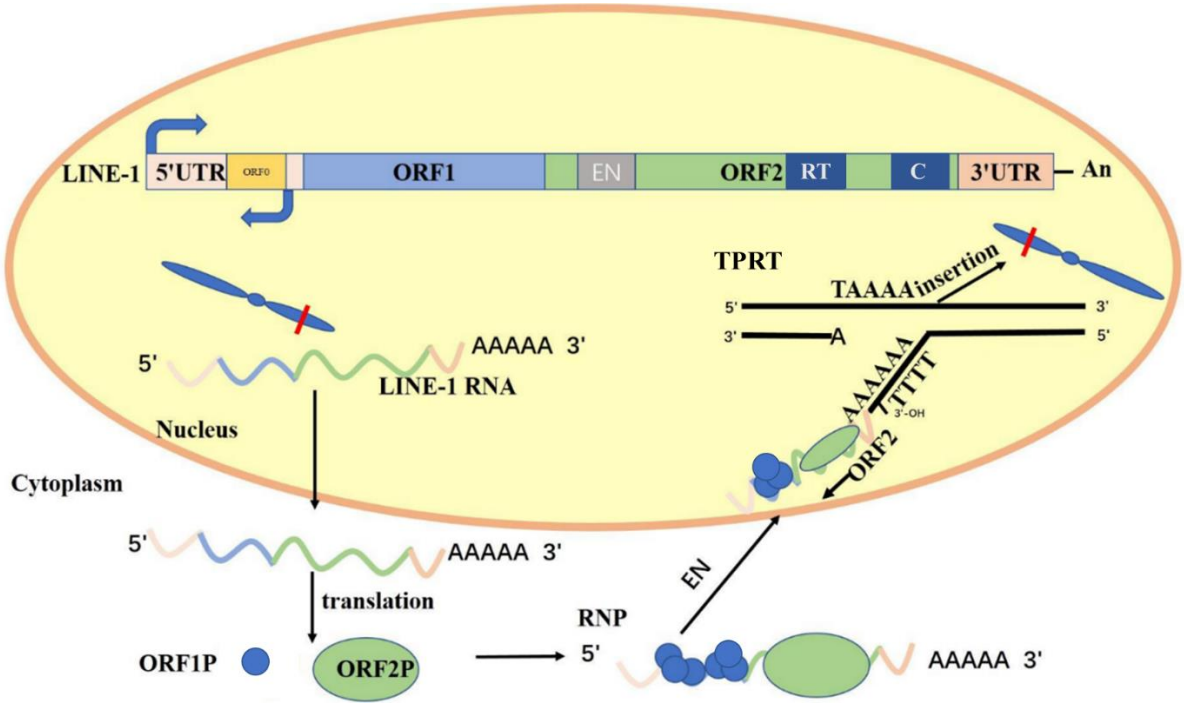

Figure 1.2: Mechanism of LINE-1 retrotransposition. A LINE-1 element consists of five different functional regions. Starting at the N-terminus the first functional region is the 5' untranslated region (UTR) containing the promoter for transcription of ORF1 and 2. The ORF0 promoter is present in the anti-sense strand of the 5' UTR. More downstream are the ORF1 exon and the ORF2 exon. The latter has an endonuclease (EN), a reverse transcriptase (RT) and a cysteine-rich domain (C). At the C-terminus, the 3' UTR ends with a poly-A tail (8). LINE-1 is transcribed to mRNA and exported to the cytoplasm. LINE-1 mRNA is translated into ORF1p and ORF2p. A ribonucleoprotein (RNP) is formed in the cytosol consisting of LINE-1 mRNA, multiple ORF1p trimers and one ORF2p. An unidentified mechanism transports the RNP back into the nucleus. The EN of ORF2p cleaves the DNA and target primed reverse transcription (TPRT) occurs where the RT transcribe the LINE-1 mRNA back into DNA. As a result, an extra copy of LINE-1 is inserted in the genome at a new location (6, 27, 28). Figure adapted from Zhang X et al, Front Cell Dev Biol., 2020, **8**, 657.

1.2 METHYL CpG BINDING PROTEIN 2

Methyl CpG binding protein 2 (MeCP2) is a protein which plays a role in the inhibition of the transcription of LINE-1. As the name indicates, MeCP2 binds to a single methylated cytosine-guanine (CpG) site in the LINE-1 promoter, which results in repressing LINE-1 transcription (37, 38).

1.2.1 MeCP2 structure

The *MeCP2* gene consist of four exons and three introns and is located on the X-chromosome (39, 40). Therefore, MeCP2 is subjected to X-chromosome inactivation (XCI) resulting in different basal MeCP2 levels between sexes (39). When genes escape XCI, biallelic expression produces more protein than monoallelic expression. The impact of XCI is not always present because of other interfering processes. Furthermore, the abundance of the MeCP2 isoforms differs between sex and type of brain cell such as neurons, astrocytes and glial cells (39).

The *MeCP2* gene is transcribed into pre-mRNA. Alternative splicing of the pre-mRNA creates two splice variants: MeCP2-E1 and MeCP2-E2. These structures are shown in Figure 1.3 (40). Due to the alternative splicing, the isoforms have their own translational start site, localised on different exons (41, 42).

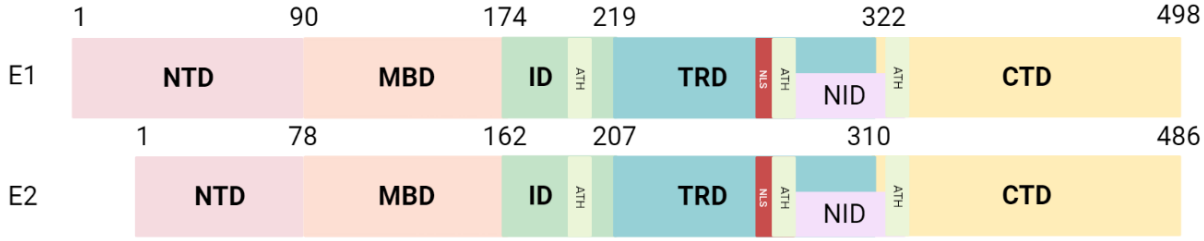

Figure 1.3: Structure of MeCP2. The functional domains of MeCP2 are the N-terminal domain (NTD), the methyl binding domain (MBD), the intervening domain (ID), the transcription repression domain (TRD) including the nuclear localization signal (NLS), the NCoR interaction domain (NID) that spans the TRD and the C-terminal domain (CTD). MeCP2 contains three AT-hooks (ATHs). Alternative splicing determines if the E1 or E2 isoform is formed. The E1 isoform exists of exons 1, 3 and 4. While, the E2 isoform is formed by exons 2,3 and 4 (43, 44). The difference between the isoforms is the longer NTD of the E1 isoform. The E1 NTD contains a poly-alanine and a poly-glycine track which are lacking in the E2 isoform. (45). The figure is adapted with Biorender from: Good KV et al, Front Genet., 2021, **12**, 620859.

MeCP2 contains several functional domains which are clearly defined. Going from the N-terminus to the C-terminus, there is the N-terminal domain (NTD), methyl binding domain (MBD), intervening domain (ID), and transcription repression domain (TRD). The TRD includes the nuclear localization signal (NLS) and particularly the NCoR interaction domain (NID). The NID spans from aa 285 to 313 localised in the TRD and the C-terminal domain (CTD) (43, 44). MeCP2 has three AT-hooks (ATHs). ATHs contain the specific amino acids motive GRP. This motive is surrounded by basic amino acids. ATHs bind in the minor groove of DNA, resulting in an amended major groove and an altered DNA structure (44, 46). The first ATH of MeCP2 is located in the ID around aa 184-195.

The second ATH, which contains aa 264 to 273, is located partially in the NLS (aa 253-271) inside the TRD of MeCP2 (43, 44). Mutation in this ATH affects MeCP2 binding to DNA and the densification of chromatin (44, 46, 47). The third ATH is at aa 295-313 in the CTD (44). Apart from the primary structure of MeCP2, which contains several functional domains, there are not many secondary or tertiary structures in MeCP2 since the protein is mostly disordered. Remarkably, more indels are found in these disordered regions (40, 43).

1.2.2 MeCP2 isoforms

There are two isoforms of MeCP2. MeCP2-E1 is 498 aa long and is transcribed from exons 1, 3 and 4, whereas MeCP2-E2 has a length of 486 aa and is formed by exons 2, 3 and 4 (40, 42, 48). Moreover, E1 is the ancestral form of MeCP2 (45). This isoform is found in all vertebrates, in contrast to the E2 isoform, which is only found in mammals (48).

The only structural difference between the isoforms is a 12 aa polyalanine track at the N-terminus (40). This track is lacking in the N-terminus of the E2 isoform, which only exists of 9 aa, in comparison with the 21 aa in the N-terminus of the E1 isoform (40, 48). The E1 isoform is degraded faster than the E2 isoform due to the difference in the N-terminus (45, 49).

Although both isoforms of MeCP2 show functional overlap, they do not fully compensate for each other. Only mutations in E1 lead to a Rett syndrome (RTT)-like phenotype in a mouse model. Still, overexpression of E2 to the amount of E1 can rescue RTT-like symptoms in RTT mouse models. Further research has to determine if the lower endogenous expression levels of E2, a different functionality of the isoforms or a different cellular distribution cause this phenomenon (45, 48). A study by Martínez De Paz et al. revealed that the E1 and E2 isoform are involved in similar cellular processes such as RNA processing, chromatin control and microtubule regulation. Because of different protein interaction partners, the specific role of the isoforms in the same process may differ (45).

Additionally, MeCP2 binds to methylated DNA (50). However, the specific interactions with DNA differ between the E1 and the E2 isoform. E1 has lower structural stability and lower binding affinity for non- and methylated genomic DNA. The E1 isoform binds to DNA with hydrogen bonds and electrostatic interactions, whereas the E2 isoform mainly binds via unspecific interactions such as hydrophobic desolvation and steric arrangements (40).

MeCP2 is widely distributed in the brain (48, 51, 52) and the isoforms are distinctly expressed in different brain regions (45, 48, 52). The abundance of E1 is evenly spread over several mouse brain regions, such as the olfactory bulb, striatum, cortex, hippocampus, thalamus, brain stem and the cerebellum. In contrast to the E1 isoform, the E2 isoform is not uniformly distributed throughout these brain regions. The striatum, thalamus and brain stem have significantly lower E2 levels than E1 levels

(52). Besides, the MeCP2-E2 isoform was discovered first and is 10 to 15 times less expressed in the brain than the E1 isoform (40, 43, 45, 48). Moreover, the expression of MeCP2-E1 in the developing brain starts earlier than that of MeCP2-E2 (45, 48, 52).

1.2.3 MeCP2 function

Methylation and deamination of CpG-cytosine to thymine are two methods for inactivating TEs (53). DNA methylation has a main role in the silencing of genes, formation of heterochromatin, XCI, genomic imprinting and inhibition of transcription of retroviral elements (53, 54, 55). Cytosine is the nucleobase which gets methylated at a CpG site. Moreover, up to 1% of the cytosines in the genome are methylated. A methyl group on a cytosine is transferred by DNA methyl transferases to create 5-methylated cytosine. Removal of DNA methylation tags results in a 5-hydroxymethylated cytosine intermediate or a thymine intermediate.

Besides enzymes that write or erase methylation tags, there is an epigenetic group of proteins such as MeCP2 that read methylation tags (53, 56). In addition, the CpG sites in the LINE-1 promoter can be methylated and therefore, the LINE-1 promoter is regulated by MeCP2 (4, 37).

MeCP2 can act as a transcriptional repressor or activator, dependent on the binding of different co-factors, as shown in Figure 1.4 (57, 58). To form a transcriptional repressor complex, mSin3a binds to the TRD of MeCP2 and mSin3a recruits histone deacetylase (HDAC) resulting in repressed transcription (38, 41, 59). However, when MeCP2 binds cAMP response element binding protein 1, a transcriptional activator complex is formed. The presence of a co-activator protein cannot be excluded (41, 57, 60).

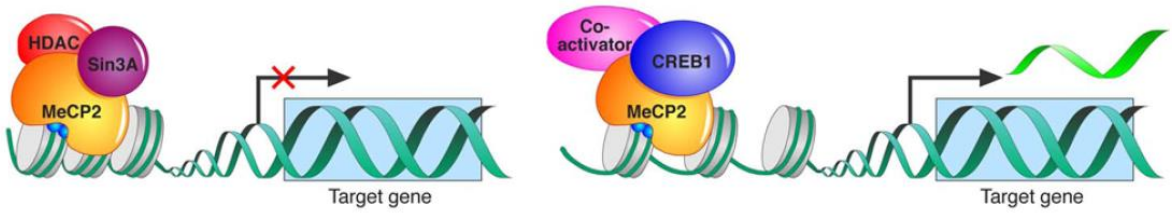

Figure 1.4: MeCP2 as a transcriptional inhibitor or activator. MeCP2 recruits Sin3A and histone deacetylase (HDAC) to repress the transcription of the target gene. MeCP2 binds to cAMP response element binding protein 1. The presence of a co-activator to the MeCP2-cAMP response element binding protein 1 complex to create the transcriptional activator complex is not excluded. MeCP2 binds to CpG sites on the promoter (in blue) (57). The figure is taken from: Chahrour S. et al, science, 2008, **320**, 1224-1229.

MeCP2 binds to the methylated promoter of LINE-1 via the MBD to inactivate transcription (4, 37, 41, 53), whereas the TRD and CTD bind DNA in a sequence independent way (41). Muotri et al. showed in *MeCP2* knockout (KO) mice that the striatum, cerebellum, hippocampus, cortex and olfactory bulb are more susceptible to LINE-1 retrotransposition than other brain regions. Additionally, this study showed that RTT patients have an increase of the ORF2 sequences in the brain compared with heart tissue

from the same patients (37). Another study by Coufal et al., revealed a higher presence of LINE-1 elements in neuronal tissue compared with non-neuronal tissue (61).

MeCP2 does not only recognise DNA methylation tags, but also histone methylation tags (4, 40, 43). The MBD of MeCP2 recognises the trimethylated lysine 27 of histone 3 (H3K27me3), an epigenetic transcriptional repressive mark on histones. Binding between MeCP2 and H3K27me3 results in heterochromatin formation (50, 54, 62). H3K27me3 and 5-methylated cytosine probably compete for binding with MeCP2 (50).

1.3 LENS EPITHELIUM-DERIVED GROWTH FACTOR

1.3.1 Structure of LEDGF

The PC4- and SFRS1- interacting protein 1 *(PSIP1)* gene located on chromosome 9 encodes for the lens epithelium-derived growth factor (LEDGF) protein. This protein has two splice variants, LEDGF/p75 and LEDGF/p52 (63, 64, 65). The names p75 and p52 originate from the protein mass in kDa (66). Both isoforms share the same N-terminus, but the C-terminus differs as a result of alternative splicing. LEDGF/p75 and LEDGF/p52 have a proline-tryptophan-tryptophan-proline (PWWP) domain, an NLS, two ATHs and three charged regions (CRs) in common. The C-terminus of LEDGF varies between the isoforms in the presence or absence of an integrase binding domain (IBD). The C-terminus or carboxy-terminal tail (CTT) of LEDGF/p52 counts 8 aa instead of the LEDGF/p75 C-terminus which contains 205 aa. Moreover, LEDGF/p75 is unstructured besides the IBD (58, 63, 65, 66). The structures of LEDGF/p75 and LEDGF/p52 are shown in Figure 1.5 (65).

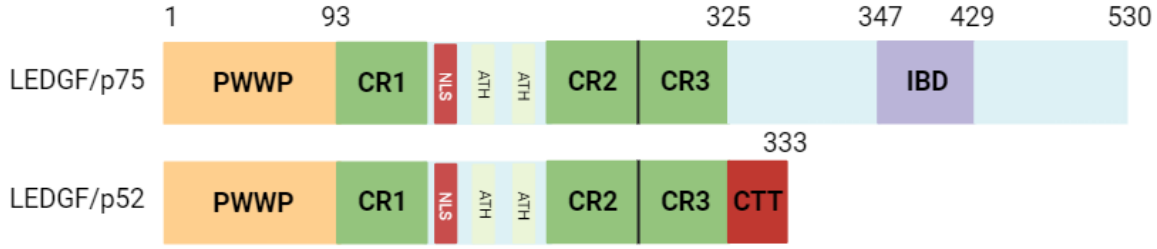

Figure 1.5: The structure of LEDGF/p75 and LEDGF/52. LEDGF/p75 and LEDGF/p52 have a common N-terminus existing of a pro-trp-trp-pro (PWWP) domain, three charged regions (CRs), a nuclear localisation signal (NLS) and an AT-hook (ATH). LEDGF/p52 has a carboxy-terminal tail (CTT) in contrast to LEDGF/p75 which has an integrase binding domain (IBD). Figure adapted with Biorender from: Ortiz-Hernandez GL et al, 2020, **11**(1).

1.3.2 Function of LEDGF

LEDGF/p75 is mostly known as a molecular tether of the human immunodeficiency virus (HIV) integrase towards the human genome (64, 65, 67, 68). The C-terminal IBD of LEDGF/p75 binds to the HIV integrase domain (69, 70, 71) and the N-terminal PWWP domain binds to methylated nucleosome tags in euchromatin such as H3K36me2 and 3 (67, 68, 71). LEDGF/p75 tethers the HIV genome for

integration towards euchromatin. For this reason, the HIV provirus is integrated into actively transcribed genes resulting in an effective replication of the virus (68).

The IBD is absent in the p52 splice variant. Therefore, this isoform is not involved in the integration of HIV in the genome (66). However, LEDGF/p52 binds as well to the epigenetically modulated nucleosomes at H3K36me3 (72). H3K36me3 nucleosomes are enhanced at highly expressed exons. LEDGF/p52 recruits alternative splicing factors such as Serine arginine-Rich Splicing Factor 1 (1, 72). As a conclusion, this suggests a role of LEDGF/p52 in mRNA splicing.

1.3.3 LEDGF interacts with MeCP2

In 2012, Leoh et al. found that LEDGF interacts with MeCP2 (58). The interaction of MeCP2 with LEDGF/p75 upregulates the expression of the Hsp27 promoter, in contrast to LEDGF/p52 which represses the Hsp27 promoter. Both LEDGF isoforms bind to MeCP2 by means of the N-terminal PWWP-CR1-domain (58). Li et al. confirmed this interaction in a mouse brain (1). According to this study, LEDGF/p52 binds to aa 270-294 of MeCP2, localised in the NID inside the TRD (1, 41). Common RTT-causing MeCP2 mutations in the TRD such as R270X and R294X can destroy the binding to LEDGF/p52 (1, 56).

1.4 LINE-1 AS A POTENTIAL PATHOGENIC FACTOR IN SEVERAL DISEASES

LINE-1 is a retrotransposon that can play a role in the onset of different diseases since it may induce DNA damage (8, 29). Therefore, gene disruption caused by TPRT can have serious implications (8, 20). A correlation between LINE-1 activity and cancer, metabolic disorders, neurological disorders, genetic disorders and autoimmune diseases has been found. In those cases, the LINE-1 promoter is hypomethylated (20). RTT and MeCP2 duplication syndrome (MDS) are LINE-1-associated brain disorders and even ageing is associated with increased LINE-1 retrotransposition (8).

1.4.1 Rett syndrome

In normal circumstances, functional MeCP2 can be a transcriptional repressor of LINE-1. Muotri et al. found enhanced LINE-1 retrotransposition in RTT patients which have a loss of function mutations in MeCP2 (37).

De novo loss of function mutations of the *MeCP2* gene are the main cause for the onset of RTT (48). Nevertheless, XCI is the main maternal way of inheriting and passing the mutation to the offspring (43, 52). This means that girls (XX-karyotype) or boys, having Klinefelter syndrome (XXY-karyotype), have a mutated X-chromosome. Those patients have a milder phenotype than boys (XY-karyotype) because the mutation in one of the X-chromosomes is compensated by the healthy X-chromosome (43, 56).

A child with RTT develops in a normal way up to the age of six months to two years (43, 48, 73). The first symptoms are subtle like muscle hypotonia, general motor impairment, and delayed growth.

With time, the neurodevelopmental disease evolves to stereotyped handwringing, lack of coordinated motions, mental retardation, breath holding, and autism-like characteristics. (40). At an older age, those patients also develop cardiac arrhythmias and seizures (48).

There are 4600 mutations known in the *MeCP2* gene, of which 70% are causing RTT. Eight of these mutations account for 47% of the main occurring mutations. Missense mutations in the MBD are the most common RTT-causing mutations. Three common mutations in the MBD are R106W, R133C and T158M. The main mutation in the ID is the R168X mutation. The TRD has four common mutations: R255X, R270X, R306X and R294X (48). However, mutations in other functional domains affect the function of MeCP2. Mutations in the NTD affect, through the MBD, the DNA binding ability and the turnover rate of MeCP2. On the other hand, mutations in the CTD influence the interactions between MeCP2, chromatin and RNA (43).

1.4.2 MeCP2 duplication syndrome

When MeCP2 is overexpressed, as a result of a 430 kb duplication at the Xq28 region, patients suffer from MeCP2 duplication syndrome (MDS) (48, 56, 74). Patients with MDS display neurodevelopmental delay, hypotonia, epilepsy, motor dysfunction and autistic behaviour such as RTT patients (74). However, the neurodevelopmental disorder symptoms occur later in this disease (74, 75). In contrast to RTT, MDS patients are mostly male (74, 75). Remarkably, MDS is characterised by an immunodeficiency resulting in frequent lung infections (75). Besides a duplication, a triplication of the *MeCP2* gene also exists. Those patients have even more severe symptoms and die earlier (76).

The levels of MeCP2 should be kept between physiological amounts (48, 75). MDS should be easier to treat than RTT because reducing the excess of MeCP2 is easier than increasing the MeCP2 level. However, over-correcting MeCP2 in MDS can create RTT and increasing MeCP2 in RTT can cause MDS. Hence the need for sensitive, selective, specific and non-invasive biomarkers to measure the MeCP2 levels and adapt the treatment to the needs of the patient (75).

1.4.3 Ageing

It is well known that LINE-1 retrotransposition increases during ageing (8). During cellular senescence, cellular factors perform no longer their endogenous function (29). Cellular senescence is an irreversible cell cycle arrest evoked by stress, resulting in a phenotypic transformation of cells (29, 77). LINE-1 senescence activation is dependent on Retinoblastoma protein (RB1), three-prime repair exonuclease 1 (TREX1) and forkhead box protein A1 (FOXA1) (29, 32, 78, 79). During cellular senescence, RB1 and TREX1 expression levels decrease. To begin with RB1, RB1 repress LINE-1 transcription via transferring the euchromatin into heterochromatin, because RB1 binds to repetitive motives such as LINE-1 elements (78). The second important protein is TREX1. The 3’ exonuclease of TREX1 breaks down free

single- and double-stranded DNA in the cytosol, including free cytosolic LINE-1 DNA (79, 80). It needs to be further investigated how free LINE-1 DNA ends up in the cytosol. Thomas et al. suggested two possible theories (79). The first theory supposes that TPRT occurs already in the cytosol when there is an excess of LINE-1 mRNA and LINE-1 derived proteins. The second proposed theory claims that unsuccessful TPRT results in a loose single-stranded DNA that is transported out of the nucleus, via an unknown mechanism (79). Finally, FOXA1 is a transcriptional activator which is upregulated in senescent cells. FOXA1 binds to the 5' UTR of a LINE-1 element and increases expression of the sense and antisense LINE-1 promotor. Taken all together, the change in the expression of RB1, TREX1 and FOXA1 promotes LINE-1 activation in senescent cells (78).

Sirtuin 6 (SIRT6) is a protein deacetylase and mono-ADP ribosyltransferase that is related to non-senescence mechanisms (8, 29). SIRT6 binds to the 5' UTR to promote LINE-1 silencing (29). Upon ageing, more DNA damage occurs and SIRT6 repairs those DNA damage sites. Therefore, SIRT6 has to alter its position from the 5' UTR of LINE-1 to the damaged DNA site. The repressing activity on the LINE-1 promoter is being abolished which results in higher LINE-1 retrotransposition events (81). SIRT6 also interacts with heterochromatin-forming proteins such as MeCP2 and KRAB-associated protein 1 (KAP1) (8, 29, 81). KAP1 is a multifunctional protein and the function is determined by its post-translational modifications. (29). The mono-ADP ribosyltransferase domain of SIRT6 reacts with KAP1 resulting in mono-ADP ribosylated KAP1 that interacts again with SIRT6 to repress LINE-1 transcription via the condensation of the 5' UTR (8, 29, 81).

The regulation of LINE-1 retrotransposition and the influences thereof are a complex multifactorial interplay between proteins. The effects of LINE-1 retrotransposition are not fully disclosed yet. Therefore, revealing and understanding one of the diverse factors increases our insights into the retrotransposition process and the effects thereof.

2 RESEARCH OBJECTIVES

The LINE-1 promoter is regulated by binding of MeCP2, while the transcriptional activator or repressor activity of MeCP2 is determined by binding of several proteins. The interaction between MeCP2 and LEDGF is found in HEK293T cells and in mice brains (1, 58).

The scope of this master's thesis is to get a better understanding of the interaction between MeCP2 and LEDGF on the LINE-1 promoter *in vitro*. And to get an indicative insight if LEDGF influence the expression level of MeCP2 *in vivo*.

According to the hypothesis, a KO of the *PSIP1* gene creates a MeCP2 driven transcriptional repressor complex. The expression of genes regulated by the MeCP2 repressor complex will be decreased. Creating a KO of the *MeCP2* gene prohibits the formation of the transcriptional repressor complex, resulting in an increase in gene expression. The hypothesis of the regulation of the LINE-1 promoter is illustrated in Figure 2.1. The interface of the Venn diagram represents the subset of genes, which are upregulated in a *MeCP2* KO cell and downregulated in a *PSIP1* KO cell. This subset are genes of which the transcription is regulated by MeCP2 and LEDGF. In accordance with the hypothesis, LINE-1 is hopefully identified in the subset of genes.

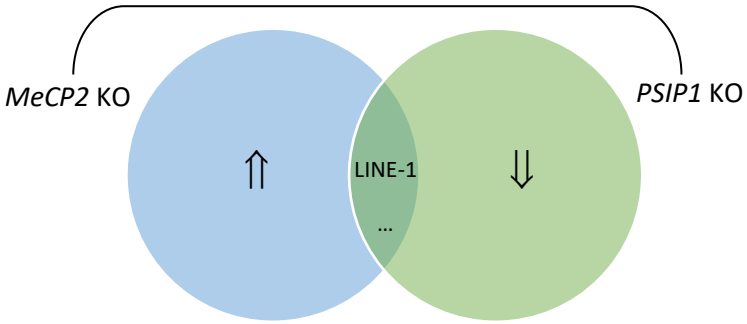

Figure 2.1: Venn diagram of expected alteration in gene expression. The blue circle represents the genes that are upregulated when there is a KO of the *MeCP2* gene. The green circle represents the genes that are downregulated when there is a KO of *PSIP1* gene. The interface is formed by the genes that follow this specific pattern of gene expression regulation. According to the hypothesis, LINE-1 will hopefully be identified in the interface.

In the first part of this master's thesis, the interaction between the two proteins, MeCP2 and LEDGF, on the LINE-1 promoter will be studied *in vitro*. The first objective is to create a KO of the *PSIP1* gene or *MeCP2* gene via a transduction of HEK293T cells with virus-like particles (VLPs). Afterwards, the KO cell lines will be validated.

In the second part of this master's thesis, the influence of LEDGF on the MeCP2 protein levels will be studied *in vivo*. Previous research in our lab showed an altered MeCP2 expression level in a conditional *PSIP1* KO mouse model in the brain. In this master's thesis, the influence of a local, brain region specific *PSIP1* KO on the MeCP2 protein levels will be studied. To induce the local *PSIP1* KO in a mouse brain, *PSIP1*$^{fl/fl}$ C57BL/6J mice will be stereotactically injected with a CMViesynapsin-intron-Cre adeno-associated virus-based (AAV) vector 2/7 (82, 83). The brain regions that will be studied are the substantia nigra (SN), ventral tegmental area (VTA), striatum, hippocampus and cortex. First, the local created *PSIP1* KO will be validated. Secondly, the possible impact of the local *PSIP1* KO on MeCP2 protein levels will be determined.

3 MATERIALS AND METHODS

3.1 CELL CULTURE

HEK293T cells were kept in culture in Dulbecco's modified Eagle medium (DMEM) [Gibco] containing fetal bovine serum [5%; Gibco] with gentamicin [1:1000; Gibco]. HEK293T cells were cultured at 37°C with a 5% CO_2 saturation. Cell lines were regularly tested for mycoplasma.

3.2 CONSTRUCT DESIGN AND CLONING

Four different DNA constructs encoding for a single-guide RNA (sgRNA) to KO *MeCP2* or *PSIP1* were designed. The construct was cloned into a pX321 plasmid backbone. Of the four DNA constructs, two constructs were designed to eradicate both protein isoforms of MeCP2 and two constructs to eradicate both isoforms of LEDGF. The pX321 backbone contains an *ampicillin resistance* gene, a F1 ORI and a U6 promoter region. The four sgRNA templates are under the regulation of the plasmid U6 promoter. In Table 3.1 the sequences of the constructs are shown.

Table 3.1: Overview of the used DNA constructs

Target	Forward stand (5' to 3')	Complementary strand (5' to 3')
MeCP2-construct 1	GATTGCGTACTTCGAAAAGGT	ACCTTTTCGAAGTACGCAATC
MeCP2-construct 2	GGACACGGAAGCTTAAGCAA	TTGCTTAAGCTTCCGTGTCC
LEDGF-construct 1	GAGATCGAAAACGCAAGCAAG	CTTGCTTGCGTTTTCGATCTC
LEDGF-construct 2	GACATCAGTAATCCTACCTGC	GCAGGTAGGATTACTGATGTC

3.3 VALIDATION OF SINGLE GUIDE-RNA'S

The potential of the sgRNAs to create a KO of the gene of interest has to be determined via a transfection experiment.

HEK293T cells were seeded in a 24-well plate at a density of 300 000 cells/well. One day after seeding, HEK293T cells were co-transfected with a Cas9 plasmid and one of the four DNA constructs or an enhanced green fluorescent protein (EGFP) plasmid. The transfection for one plasmid was carried out in a final volume of 50 µL OptiMEM [Gibco] transfection mix containing 3 µL Lipofectamine 3000, 1 µL p3000 reagents [Invitrogen], 750 ng Cas9 plasmid and 1 µg of the plasmid.

One day post-transfection, the cells transfected with the EGFP plasmid were fixed with a paraformaldehyde solution [4%; Merck] before counting with the flow cytometer [Thermo Fisher] to determine the transfection efficiency. While, the cells transfected with the sgRNAs for MeCP2 or LEDGF were scaled up to a 6-well plate. Two days post-transfection, genomic DNA extraction was performed according to the manufacturer's protocol [BioRad]. A polymerase chain reaction (PCR) was performed with the primers listed in Table 3.2. A Gen-Elute PCR clean-up [Sigma Aldrich] was performed and the samples were sequenced by LGC Bio research Technologies [LGC genomics; Germany] to evaluate the

degree of frameshift and non-frameshift mutations. The raw sequencing data was analysed with the online free tools ICE [Synthego Performance Analysis; ICE Analysis; 2019; v3.0; Synthego] and Decodr [Decodr; v3.0; (84)] to determine the degree of frameshift and non-frameshift mutations in the mutated cell lines.

Table 3.2: Primer DNA sequence used in the validation of the created KO cell lines

Target	Forward primer (5' to 3')	Reverse primer (5' to 3')
MeCP2-construct 1	TCTTTGGTTGCTGAACTTTGGAG	CTTTTCTCCAGGACCCTTTTCA
MeCP2-construct 2	GAAGAAAAGTCAGAAGACCAGG	CACGGTCATTTCAAGCACAC
LEDGF-construct 1	GCAGAGATAGGTGTAATTCAAAGAC	ATAATTCACAGAGTGACTGCC
LEDGF-construct 2	CGTTACCATAGACTGGCATA	CACAGCCTCTCTTACCACTA

3.4 PRODUCTION OF VIRUS-LIKE PARTICLES AND TRANSDUCTION OF HEK293TS

The production of the murine leukemia virus-based VLPs was performed according previous research of Mangeot et al. (85). The production and the transduction of HEK293T cells with those VLPs was performed by the Leuven Viral Vector Core.

3.5 WESTERN BLOT

To visualise the remaining proteins, a Western blot analysis was performed. Cells were collected and washed twice with phosphate-buffered saline (PBS) [Gibco]. The cells were lysed with RIPA buffer containing sodium dodecyl sulfate [0.1% Acros Organics], tris(hydroxymethyl)aminomethane hydrochloride [pH: 8; SAFC], sodium chloride [Sigma-Aldrich], sodium deoxycholate [0.5%; Sigma-Aldrich] and NP-40 [Thermo Fisher]. The lysed samples were kept on ice for 30 minutes and were vortexed every 10 minutes. A bicinchoninic acid (BCA) assay [Thermo Fisher] was performed to determine the total protein concentration.

Samples were loaded on a Novex tris-glycine gel [4-15%; Thermo Fisher]. After the transfer to a nitrocellulose membrane [GE Healthcare life science], the membrane was stained with Ponceau S [Sigma Aldrich] to check the equal loading of the proteins. The membrane was blocked for 30 minutes with 5% milk in PBS [Gibco] with Triton-X100 [0.1%; Acros Organics]. The membrane was incubated overnight at 4°C with primary antibodies diluted in blocking buffer. The primary polyclonal rabbit anti-LEDGF antibody [1:1000; Abcam] and the primary monoclonal rabbit anti-MeCP2 antibody [1:400; Cell Signaling] were used. The primary mouse anti-vinculin antibody [1:100 000; Sigma-Aldrich] was used to correct for equal protein loading. After washing the membrane with PBS [Gibco] with Triton-X100 [0.1%; Acros Organics], the membrane was incubated for two hours with horseradish peroxidase-conjugated goat anti-rabbit IgG secondary antibody [1:20 000; Dako] and the horseradish peroxidase-conjugated goat anti-mouse IgG secondary antibody [1:20 000; Dako]. After washing with

PBS [Gibco] with Triton-X100 [0.1%; Acros Organics] the membrane was developed using Clarify Western ECL substrate [Bio-Rad]. The blot was visualised with the detector [Amersham ImageQuant 800; Cytiva]. The quantification of the Western blot was performed with Image Lab [Bio-Rad; v6.1.0].

3.6 REVERSE TRANSCRIPTION-QUANTITATIVE POLYMERASE CHAIN REACTION

To determine the mRNA expression levels, a reverse transcription quantitative polymerase chain reaction (RT-qPCR) was performed. Cells were pelleted and washed once with PBS [Gibco]. Total RNA was extracted with the Aurum Total RNA Mini Kit [Biorad]. RNA concentrations were measured with the Nanodrop [Implen]. 5 µg of RNA was reverse transcribed into complementary DNA (cDNA) using the High-capacity cDNA Archive Kit [Applied Biosystems].

The qPCR mix contains the LightCycler 480 SYBR green I Master [Bio-Rad] and primers for MeCP2, LEDGF/p52, LEDGF/p75, or glyceraldehyde 3-phosphate dehydrogenase (GAPDH). The primer sequences are shown in Table 3.3. The qPCR was performed using the LightCycler 480 [Bio-Rad]. The GAPDH level was used to normalise the mRNA levels.

Table 3.3: primer set for qPCR

Target	Forward primer (5' to 3')	Reverse primer (5' to 3')
GAPDH	GTCTCCTCTGACTTCAACAGCG	ACCACCCTGTTGCTGTAGCCAA
MeCP2	CACGGAAGCTTAAGCAAAGG	CTGGAGCTTTGGGAGATTTG
LEDGF/p52	AACTTTCAGACTGCTCACA	GATTACATGTTGTTTGGTGC
LEDGF/p75	GAACTTGCTTCACTTCAGGTCACA	TCGCCGTATTTTTTTCAGTGTAGT

3.7 ANIMALS

C57BL/6J PSIP1-floxed (*PSIP1*$^{fl/fl}$) mice were available in the lab and were engineered to harbour LOXP sites around exon 3 of the *PSIP1* gene. The Cre-LOXP mouse model is previously described in the paper of Kos et al. (86). The *PSIP1*$^{fl/fl}$ mice were housed in filtered cages and exposed to a 12-hour light/dark cycle. The mice were fed *ad libitum* with pelleted food and had free access to tap water. All animal experiments were approved by the KU Leuven Bioethical committee [P200/2019; Belgium] and performed according to the European directive on the protection of animals used for scientific purposes [2010/63/EU].

3.8 GENOTYPING

Ear samples were taken from the 4 weeks old *PSIP1*$^{fl/fl}$ mice. The genotyping was performed according to the KAPA genotyping protocol [Roche]. A PCR band of LOXP-positive mice appeared in a DNA agarose gel at 802 bp and a band of a wild type (WT) mouse appeared at 745 bp. Primer sequences for *PSIP1* and the PCR program are shown in Table 3.4.

Table 3.4: PCR programs and primers for genotyping C57BL/6J mice

***PSIP1*-program**	**Primer set for *PSIP1* (5'-3')**
3 minutes-95°C	Forward: GAGATATCGAGGCAGAAAGAAGACTGGGATAG
15 seconds-95°C	Reverse: TGGAATTCTATCTCAAACAAACCAAAGAGC
15 seconds-55°C	
30 seconds-72°C	
10 minutes-72°C	

3.9 STEREOTACTIC INJECTIONS

PSIP1$^{fl/fl}$ mice that were eight weeks old, were injected in different brain regions with 2 µL of the CMViesynapsin-intron-Cre rAAV 2/7 vector containing 5*10^9 genome copies/mL (GC/mL). The used coordinates for injection are listed in Table 3.5. Aseptic techniques were applied during all surgical procedures. Mice were anaesthetized by intraperitoneally injection of Ketamine [Nimatek, 75 mg/kg, Dechra], and medetomidine [Dormitor, 1 mg/kg, Vetoquinol]. The anaesthetised mice were placed in a stereotactic head frame [Stoelting] and the skin was disinfected with povidone-iodine gel [10%, Iso-Betadine]. Eyes were protected with carbomer gel [Vidisic, 2 mg/g, Bausch&Lomb]. An incision was made in the scalp and a hole was drilled on the right site in the skull according to the coordinates in Table 3.5. The injections were given with a 30-gauge needle [Hamilton] at an injection speed of 0.25 µL/min. After the procedure, the wound was disinfected with povidone-iodine gel [10%, Iso-Betadine] and aipamezole [Antisedan, 5.0 mg/mL, Vetoquinol] was administered as an antidote. As post-operative analgesia Buprenorphine [Vertergesic, 30 µL/10g mice, Ceva] was given to the mouse. Xylocaine gel [2%, Aspen] was added to the wound on the skull when the mouse was in pain after surgery.

Table 3.5: Stereotactic injections in mice brains.

Area	**A/P**	**M/L**	**D**
Substantia nigra	-3.1	-1.2	-4.3
Striatum	0.5	-2.0	-3.3
Hippocampus	-1.8	-1.55	-1.9
Cortex	-1.8	-1.55	-1.0

3.10 PERFUSIONS

Four weeks after stereotactic injection, *PSIP1*$^{fl/fl}$ mice received an overdose of sodium pentobarbital [Dolethal, 60 mg/mL, Vetoquinol]. The mouse was intracardially perfused with paraformaldehyde [4%; Merck] in PBS-solution [Gibco]. The brain was collected and stored in a paraformaldehyde [4%; Merck]

diluted in PBS-solution [Gibco]. After 24 hours, the brain was stored in PBS [Gibco] with sodium azide [0.1%; Sigma Aldrich]. The full brain was sectioned with the vibratome [Thermo Scientific] in slices of 40 µm. Brain slices were stored as floating sections in a 24-well plate containing PBS [Gibco] with sodium azide [0.1%; Sigma Aldrich].

3.11 IMMUNOFLUORESCENT STAINING

Prior to staining, antigen retrieval was performed on mouse brain slices containing the striatum, hippocampus and cortex, SN and VTA. Slices were treated with citrate buffer [0.01M; pH: 6.0; Sigma-Aldrich] at 80°C for 30 minutes followed by 20 minutes on ice. Sections were blocked for one hour in 1 x PBS [Gibco] with Triton-X100 [0.1%; Acros Organics] containing goat serum [10%; Dako]. Slices were incubated overnight at room temperature with the primary antibodies diluted in blocking buffer. The used primary antibodies were: the monoclonal mouse anti-Cre antibody [1:5000; Merck], the polyclonal rabbit anti-MeCP2 antibody [1:2500; Cell Signalling] and the polyclonal rabbit anti-LEDGF/p75 [1:500; Bethyl] or the monoclonal mouse anti-LEDGF antibody [1:1000; Invitrogen]. Additional added anti-bodies were the polyclonal chicken anti-tyrosine hydroxylase (TH) primary antibody [1:1000; Aves Labs] to stain the SN and VTA. The primary polyclonal chicken anti-NeuN antibody [1:1000; Millipore] was added to stain neurons.

The next day, sections were incubated with the secondary antibodies for two hours in the dark. The secondary antibodies fluorochrome-conjugated goat anti-rabbit Alexa 488 IgG [1:500; Dako], fluorochrome-conjugated goat anti-mouse Alexa 555 IgG [1:500; Dako], fluorochrome-conjugated goat anti-chicken Alexa 633 IgG [1:500; Dako] and nuclear DAPI staining [1:2000; Invitrogen] were diluted in 1 x PBS [Gibco] with Triton-X100 [0.1%; Acros Organics]. The slices were mounted on a gelatine coated microscope slice [1%; Sigma-Aldrich]. When the slices were dry, they were incubated for 3 min with TrueBlack [Invitrogen] and rinsed with 1 x PBS [Gibco]. After drying, the slices were covered with a cover slip [1.5 µm; Menzel-Gläser] using 4-88 Mowiol [Calbiochem].

3.12 VALIDATION OF STAINING

Every staining was validated using a fluorescent microscope [Leica]. Pictures of the region of interest (ROI) were taken at a magnification of 5X. Pictures were analysed with ImageJ [NIH; (87)]. The brightness and contrast were adapted to make the cells visible.

3.13 EXPRESSION LEVELS QUANTIFICATION

Pictures for quantification were taken with a confocal microscope [LSM 880; Zeiss] at a magnification of 20X. A picture was taken, in the same slice, from the transduced region and the non-transduced region. The slices were analysed with QuPath [Windows; v0.043; (88)]. The build-in cell detection function of QuPath was used to count the cells and to measure the pixel intensity of the stained

proteins. The used parameters for cell detection with QuPath in each brain region are listed in Table 3.6. The staining with the polyclonal chicken anti-NeuN primary antibody was used to count the cells. The staining with the monoclonal mouse anti-LEDGF antibody was used to determine the *PSIP1* KO region. The staining with the polyclonal rabbit anti-MeCP2 antibody was used to detect the cells, in which the mean pixel intensity per nucleus of MeCP2 and LEDGF were measured.

Table 3.6: Parameters for cell detection in QuPath

Parameters	Striatum	Hippocampus and cortex	Ventral tegmental area and substantia nigra
Requested pixel size (µm)	0.5	0.5	0.5
Background radius (µm)	10	10	10
Median filter radius (µm)	0	0	0
Sigma (µm)	3	2.5	2.5
Minimum area (µm)	10	10	10
Maximum area (µm)	1000	1000	1000
Threshold	1	1	1
Cell expansion (µm)	2	2	2

3.14 DATA ANALYSIS

The output of QuPath was analysed with Excel [v2302; Windows] and GraphPad Prism [v9.5.1; Windows]. The mean pixel intensity per nucleus from each biological replicate were averaged and the standard deviation (SD) was additionally reported.

4 RESULTS

4.1 CREATION OF THE *IN VITRO* KNOCK-OUT OF THE *MeCP2* GENE AND *PSIP1* GENE

To achieve the first objective of this master's thesis, a CRISPR-based technique was used to produce a KO cell line of the *PSIP1* gene or the *MeCP2* gene that destroys either both protein isoforms of LEDGF or MeCP2 in HEK293T cells. The purpose of this deletion is to gain a better understanding of the interaction between MeCP2 and LEDGF on the LINE 1 promoter.

4.1.1 Validation of the sgRNAs

A transfection experiment was performed to determine, which sgRNA derived from the DNA constructs, could create the best KO of the *PSIP1* gene or *MeCP2* gene. In both experiments, HEK293T cells were transfected with a Cas9 plasmid and one of the four DNA constructs or an EGFP plasmid. One day post-transfection, samples were taken from the EGFP condition and the transfection efficiency was determined with flow cytometry. As shown in Figure 4.1, the average percentage gated EGFP-positive cells in the first transfection experiment was 78%. In the second transfection experiment, the average percentage gated EGFP positive cells was 62%.

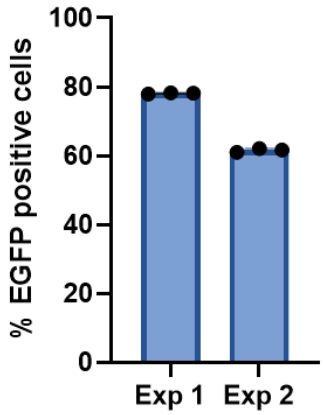

Figure 4.1: The percentage of EGFP positive cells in the two transfection experiments. HEK293T cells were co-transfected with an EGFP plasmid and a Cas9 plasmid. One day post-transfection, flow cytometry was used to determine the transfection efficiency during the validation of the sgRNAs. The first transfection experiment had a higher transfection efficiency compared to the second transfection experiment. The error bars represent the standard deviation. The analysis was performed in technical triplicate.

A genomic DNA extraction was performed from the different HEK293T cell lines. The samples were sequenced to determine the degree of the frameshift and non-frameshift mutations caused by the produced sgRNAs. By using different analysis tools, the estimated percentage of mutations differed. The raw Sanger Sequencing data was analysed by the analysing tools ICE and Decodr. ICE provides as an output the percentage of created indels including non-frameshift and frameshift mutations and a KO-score. This KO-score included the proportion of frameshift and non-frameshift mutations. The counted non-frameshift mutations were indels of 21 bp or more that occurred in an exon, which is

reasonable to create a loss-of-function mutation in a protein (89). Decodr gives as output the percentage of frameshift mutations (84). The results are shown in Table 4.1. Remarkably, the quality of the Sanger sequence data of the first transfection experiment was sometimes too low to be interpreted by Decodr. Besides, the Sanger sequencing of LEDGF-construct 2 in the second transfection experiment failed.

Table 4.1: The degree of mutation in both transfection experiments

	Transfection experiment 1			Transfection experiment 2		
Target	**ICE (% indel)**	**ICE (KO-score)**	**Decodr (% frameshift)**	**ICE (% indel)**	**ICE (KO-score)**	**Decodr (% frameshift)**
MeCP2-construct 1	32	27	32.8	0	0	6.1
MeCP2-construct 2	11	11	/	1	1	1.2
LEDGF-construct 1	18	18	22.5	1	1	9.1
LEDGF-construct 2	28	28	/	/	/	/

After evaluation of all the available data, the decision was made to continue with MeCP2-construct 1 and LEDGF-construct 2 to create VLPs. Since those constructs had the best capability to KO *PSIP1* or *MeCP2* in the first transfection experiment.

4.1.2 Validation of the created knock-out HEK293T cell line via Western blot and RT-qPCR

The VLPs were produced by the Leuven Viral Vector Core. After production, HEK293T cells were transduced with the VLPs. A week post-transduction, the *PSIP1* KO and *MeCP2* KO cells were harvested. Western blot and RT-qPCR were performed to validate the effect of the KO. Two control cell lines were made simultaneously. A *CF transmembrane conductance regulator* (CFTR) KO (90) and a scaffold VLP cell line were created as control cell lines.

Samples for Western blot and RT-qPCR were taken from all the cell lines to determine the residual MeCP2 or LEDGF expression after transduction with the VLPs. In Western blot, the equal loading was checked with staining for the housekeeping protein vinculin. Residual MeCP2 proteins were very slightly visible in the *MeCP2* KO cell line (Figure 4.2A). The Western blot quantification revealed a strong reduction of 92% in MeCP2 protein levels (Figure 4.2B). On the other hand, the RT-qPCR data showed a more subtle reduction of 32% in MeCP2 RNA levels (Figure 4.2C). Surprisingly, a decrease of LEDGF/p75 and LEDGF/p52 protein levels in the *MeCP2* KO cell line was seen in the Western blot and reported in the quantification. However, this effect is not visible in the RT-qPCR data.

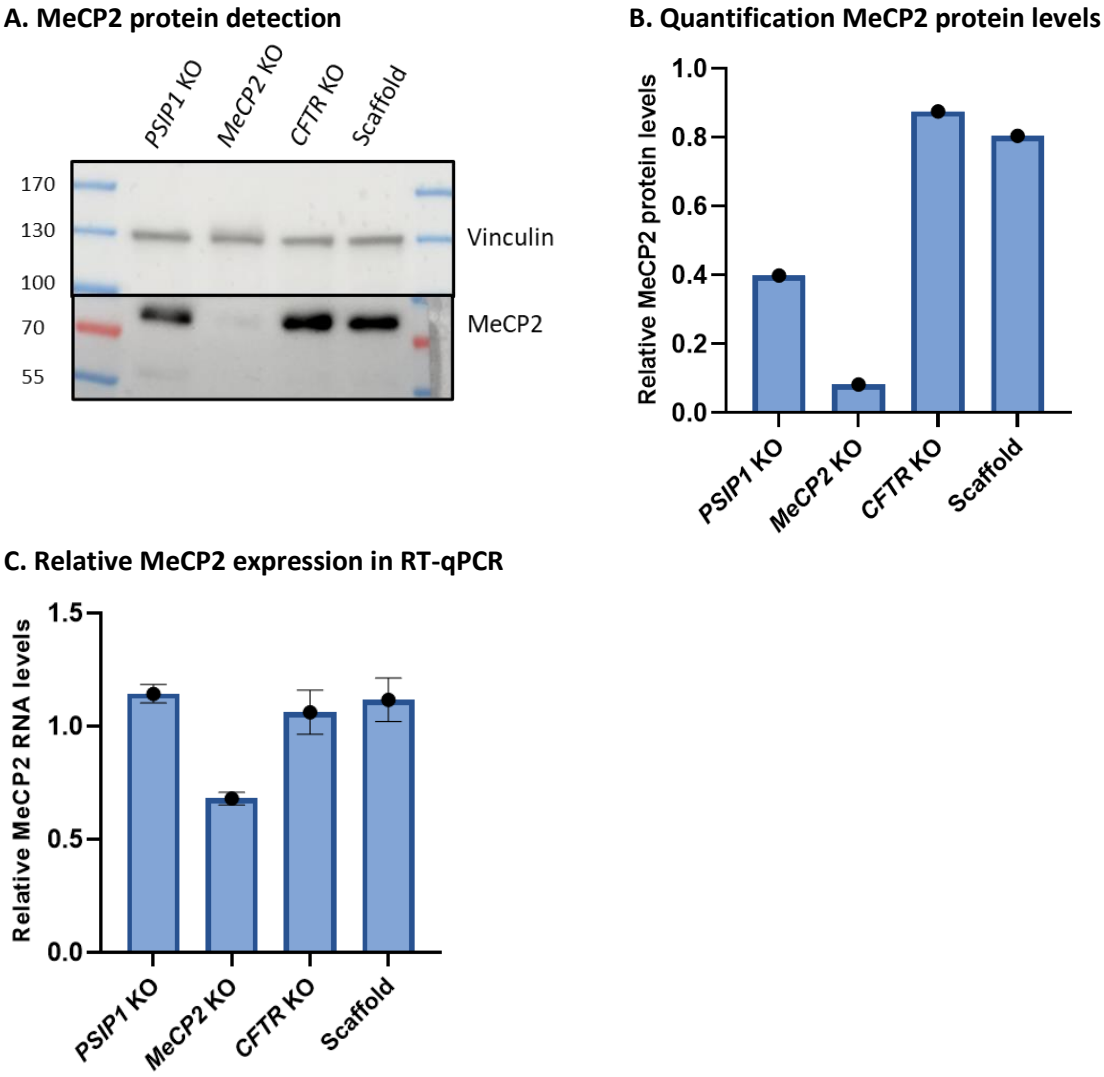

Figure 4.2: Validation of the cell lines on Western blot or RT-qPCR. A. Expression of MeCP2 and vinculin in Western blot. 30 µg of protein was loaded. The loading marker indicates kDa. Vinculin was used to control for equal loading and gives a band at a height of 130 kDa. MeCP2 was detected at a height of 75 kDa. The MeCP2 protein levels were decreased in the *MeCP2* KO and in the *PSIP1* KO cell line. The MeCP2 protein levels were equal in the *CFTR* KO and scaffold cell line. The data is obtained from one single Western blot. **B. The quantification of MeCP2 protein levels normalised to vinculin.** The MeCP2 protein levels reported in Figure 4.2A, were quantified. The values were normalised for equal loading via the housekeeping protein vinculin. **C. Relative expression of MeCP2 normalised for GAPDH in RT-qPCR.** The mRNA level of MeCP2 was normalised to GAPDH. In the *MeCP2* KO cell line, the MeCP2 RNA level was decreased. The MeCP2 RNA level was not altered in the other cell lines. The analysis was performed in technical triplicate. The standard deviation is shown in the error bars.

In Figure 4.3A, LEDGF/p75 and LEDGF/p52 proteins were not visible anymore in the *PSIP1* KO cell line. The quantification of the Western blot, shown in Figures 4.3B and C, confirms the reported findings. A reduction of 99.9% was obtained for LEDGF/p75 and a reduction of 99.2% was obtained for LEDGF/p52. Similarly, the RT-qPCR reported a reduction of 93% in RNA levels for LEDGF/p75 and for LEDGF/p52 (Figures 4.3D and E). What stands out in Figures 4.3A-C is that the MeCP2 protein level was slightly

reduced in the *PSIP1* KO cell line. The band, which slightly appears at 55 kDa, is due to non-specific binding of the anti-LEDGF antibody.

A. LEDGF/p75 and LEDGF/p52 protein detection

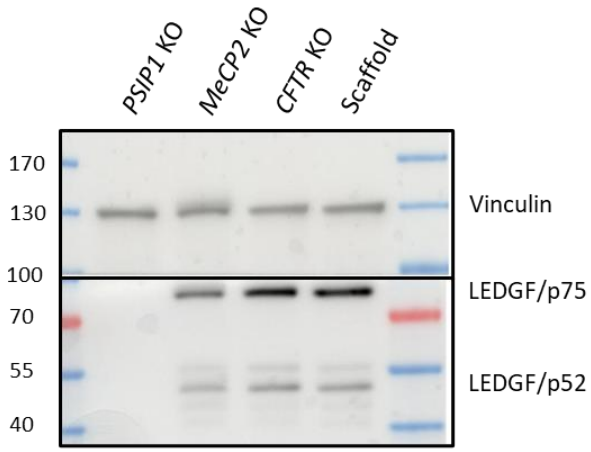

B. Quantificaton of LEDGF/p75 protein levels

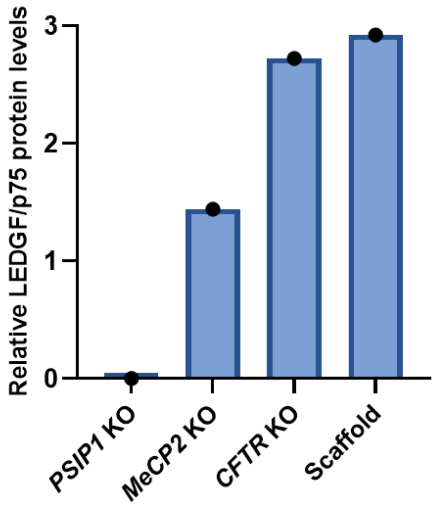

C. Quantification LEDGF/p52 protein levels

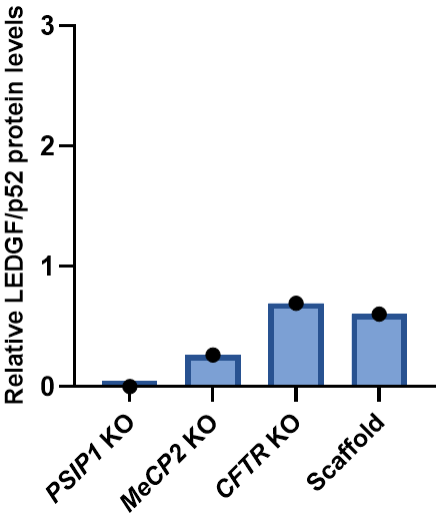

D. Relative LEDGF/p75 expression in RT-qPCR

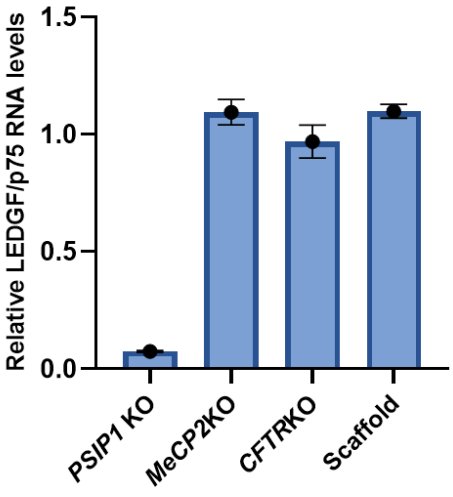

E. Relative LEDGF/p52 expression in RT-qPCR

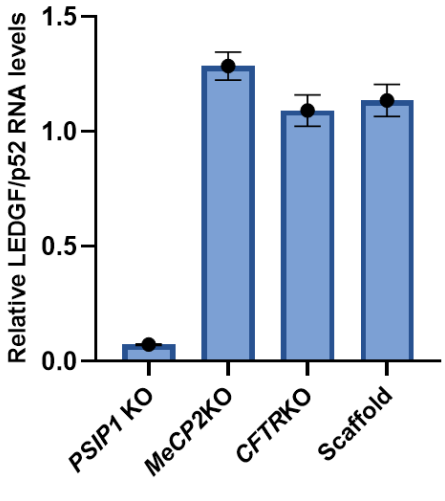

Figure 4.3: Validation of the *PSIP1* KO cell line on Western blot and RT-qPCR. A. Expression of LEDGF/p75, LEDGF/p52 and vinculin on Western blot. 30 µg of protein was loaded. The loading marker indicates kDa. Vinculin was used to control for equal loading and gives a band around 130 kDa. LEDGF/p75 gives a band at a height of 75 kDa and LEDGF/p52 was detected at a height of 52 kDa. The LEDGF/p75 and LEDGF/p52 proteins were not detectable anymore in the *PSIP1* KO cell line. The LEDGF/p75 and LEDGF/p52 protein expression was lower in the *MeCP2* KO cell line. The LEDGF/p75 and LEDGF/p52 protein levels were equal in the *CFTR* KO and scaffold cell line. The data was derived from one single Western blot. **B. The quantification of LEDGF/p75 protein levels normalised to vinculin.** The LEDGF/p75 protein levels, reported in Figure 4.3A, were quantified. The values were normalised for equal loading via the housekeeping protein vinculin. **C. The quantification of LEDGF/p52 protein levels normalised to vinculin.** The LEDGF/p52 protein levels, reported in Figure 4.3A, were quantified. The values were normalised for equal loading via the housekeeping protein vinculin. **D. Relative expression of LEDGF/p75 normalised for GAPDH in RT-qPCR.** The mRNA level of LEDGF/p75 was normalised to GAPDH. In the *PSIP1* KO cell line, the LEDGF/p75 RNA levels were decreased. The LEDGF RNA level was not altered in the other cell lines. The analysis was performed in technical triplicate. The error bars represent the standard deviation. **E. Relative expression of LEDGF/p52 normalised for GAPDH in RT-qPCR.** The mRNA level of LEDGF/p52 was normalised to GAPDH. In the *PSIP1* KO cell line, the LEDGF/p52 RNA levels were decreased. The LEDGF RNA level was not altered in the other cell lines. The analysis was performed in technical triplicate. The error bars represent the standard deviation.

4.1.3 Validation of the *PSIP1* knock-out cell line via sequencing

The *PSIP1* KO cell line was further validated by determining the KO-score and the degree of frameshift with the analysing tool ICE and Decodr (Table 4.2). A genomic DNA extraction was performed on the *PSIP1* KO cell line and the sample was sequenced. The obtained results from the analysing tool ICE, showed that 96% of the cells created an indel, with a corresponding KO-score of 94. Similarly, Decodr reported that 96% the cells generated a frameshift mutation.

Table 4.2: The degree of mutations in the PSIP1 KO cell line

Target	ICE (% indel)	ICE (KO-score)	Decodr (% frameshift)
PSIP1 gene	96	94	96

4.2 LOCAL KNOCK-OUT OF THE *PSIP1* GENE *IN VIVO*

The second objective of this master's thesis is to determine the influence of a *PSIP1* KO on MeCP2 protein levels *in vivo*.

4.2.1 Genotyping mice

Before stereotactic injections were performed, mice were genotyped to distinguish the WT C57BL/6J mice from the *PSIP1*$^{fl/fl}$ C57BL/6J mice. The mice which have a DNA band at 802 bp were identified as *PSIP1*$^{fl/fl}$ mice and used for stereotactic injections in the different brain regions with the

CMViesynapsin-intron-Cre rAAV 2/7 vector, from now on referred as Cre vector. The electrophoresis gel is shown in Figure 4.4. Mouse 1-7 were identified as *PSIP1*$^{fl/fl}$ mice.

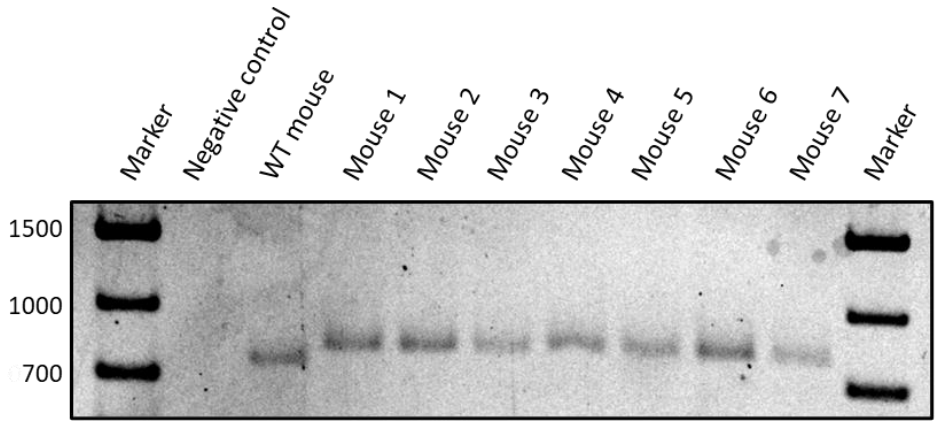

Figure 4.4: Ethidium bromide-stained electrophorese gel of *PSIP1* gene. Mice were genotyped by performing a PCR reaction with *PSIP1* specific primers. Afterwards samples were loaded on a 2% agarose gel. A negative control (water) and a WT mouse were included. The DNA marker indicates bp.

4.2.2 Validation of the transduction with the CMViesynapsin-intron-Cre rAAV 2/7 vector

The unilateral stereotactic injections with the Cre vector, were performed in biological duplicate in the striatum or hippocampus and cortex. The injections in the SN were performed in biological triplicate. A series of four technical replicates were taken through the ROI to measure the effect of the transduction with the Cre vector on the LEDGF and MeCP2 protein levels. However, three technical replicates were obtained in the hippocampus of mouse 2 since the Cre vector did not spread sufficiently throughout the whole hippocampus.

As can be seen in Figure 4.5, the Cre vector targets specific subregions inside the ROI. The hippocampus consists of different layers. The viral vector targeted the CA1-layer of the hippocampus and additionally layer 6 of the cortex in mouse 1 and 2. Mouse 3 and 4 were successfully injected in the striatum (dorsal area). Mouse 5, 6 and 7 received stereotactic injections in the SN pars compacta. The VTA was additionally completely targeted with those injections. In the regions were the Cre vector came to expression, no LEDGF proteins were visible anymore.

The dopaminergic region was defined as the VTA and SN pars compacta and stained with the polyclonal chicken anti-TH antibody to visualise specifically the dopaminergic neurons. The striatum, hippocampus and cortex were stained with the polyclonal chicken anti-NeuN antibody, to identify the neurons. All the regions were stained with the monoclonal mouse anti-Cre antibody to identify the Cre expression in the targeted regions and the polyclonal rabbit anti-LEDGF/p75 antibody to determine the LEDGF protein expression in the transduced and non-transduced area.

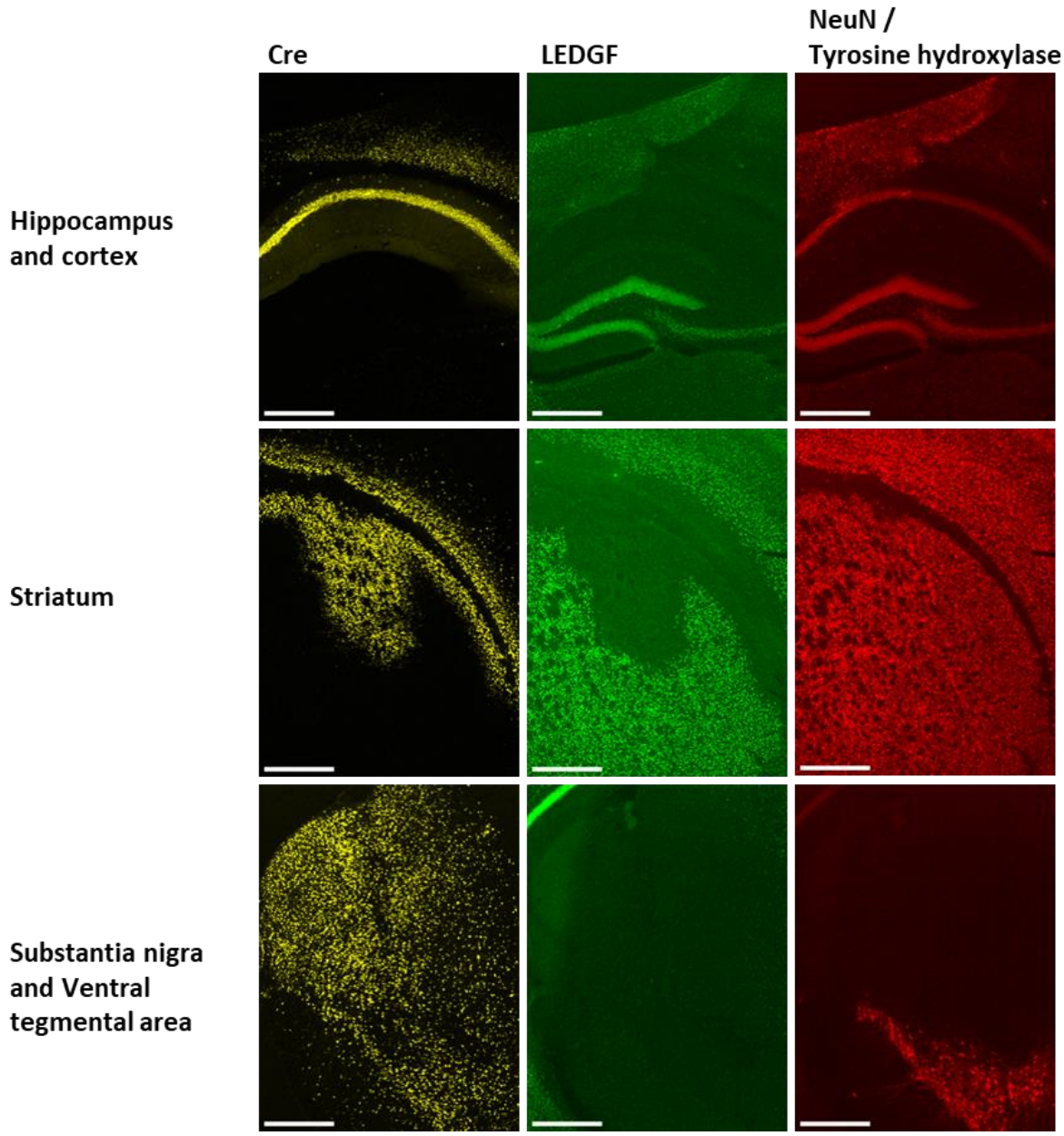

Figure 4.5: Visual validation of the Cre enzyme expression targeting the region of interest. Antigen retrieval with citrate buffer was performed. Afterwards, staining for the primary monoclonal mouse anti-Cre antibody and the secondary fluorochrome-conjugated goat anti-mouse Alexa 555 IgG antibody was added to visualise the Cre enzyme. In addition, the primary polyclonal rabbit anti-LEDGF antibody with the secondary fluorochrome-conjugated goat anti-rabbit Alexa 488 IgG was added to determine the LEDGF/p75 expression. The non-dopaminergic regions of interest were additionally stained with the primary polyclonal chicken anti-NeuN and the secondary fluorochrome-conjugated goat anti-chicken Alexa 633 IgG to indicate the neurons. The dopaminergic regions (SN and VTA) were stained with the polyclonal chicken anti-TH antibody and the secondary fluorochrome-conjugated goat anti-chicken Alexa 633 IgG to indicate the dopaminergic neurons in the region of interest. The slices were mounted with Mowiol and a cover slip. The pictures were taken with a fluorescent microscope. Magnification = 5X. Scale bar = 500 µm.

4.2.3 Validation of the *PSIP1* gene knock-out in the transduced region

The different brain regions were stained with the primary monoclonal mouse anti-LEDGF and the monoclonal rabbit anti-MeCP2 antibody. A nuclear DAPI staining was also included. In the dopaminergic regions, the polyclonal chicken anti-TH antibody was added. The results of the hippocampus, cortex and striatum are comparable because the staining was done in the same experiment. However, the results from the SN and VTA are performed in another experiment and the settings for the confocal microscope had to be adjusted. Due to an unknown artefact, the values in the cortex differs between the biological replicates. The interpretation of the individual data between mice and other brain regions has to be done carefully. Therefore, the ratio was taken to be able to compare the reduction in LEDGF and MeCP2.

The hippocampus is a representative region to show the staining in the non-dopaminergic neurons and the SN represents the dopaminergic regions. As shown in Figures 4.6 and 4.7, LEDGF proteins were visible in the non-transduced area. On the other hand, the staining shows a reduction in LEDGF/p75 and LEDGF/p52 protein expression in the transduced areas. The DAPI staining, and in the case of dopaminergic neurons, the anti-TH staining, looks similar between the non-transduced and transduced regions.

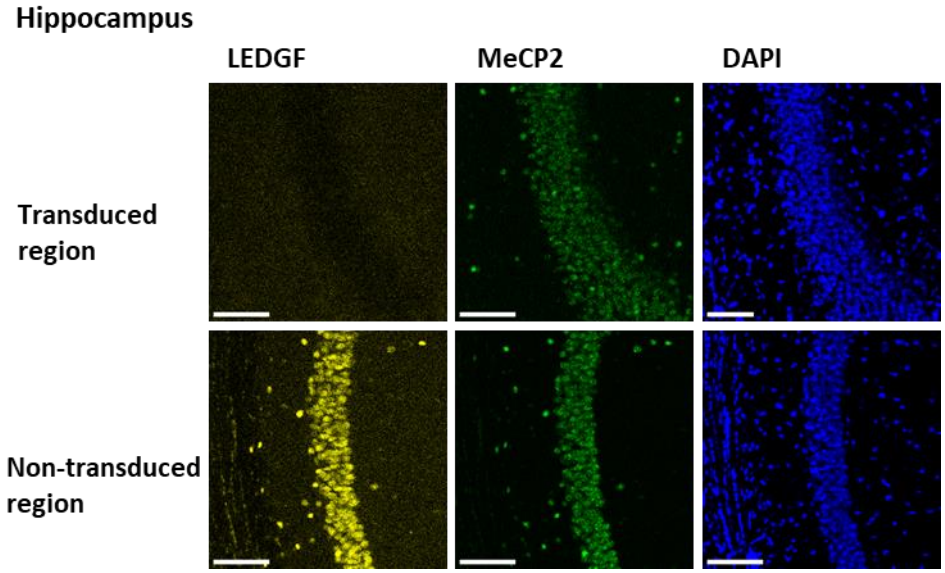

Figure 4.6: Validation of the *PSIP1* KO and effect on the MeCP2 protein levels in the hippocampus-CA1. Brain slices of the transduced region and non-transduced region are shown. Antigen retrieval with citrate buffer was performed before incubation with the monoclonal mouse anti-LEDGF antibody, which stains both LEDGF isoforms. Fluorochrome-conjugated anti-mouse Alexa 555 IgG was used as a secondary antibody. The brain slices were stained with the polyclonal rabbit anti MeCP2 antibody and the secondary antibody fluorochrome-conjugated anti-rabbit Alexa 488 IgG was used. The nuclear DAPI staining was additionally added and the slices were mounted with a cover slip and Mowiol. Pictures were taken with the confocal microscope. Magnification = 20X. The scale bar = 100 µm.

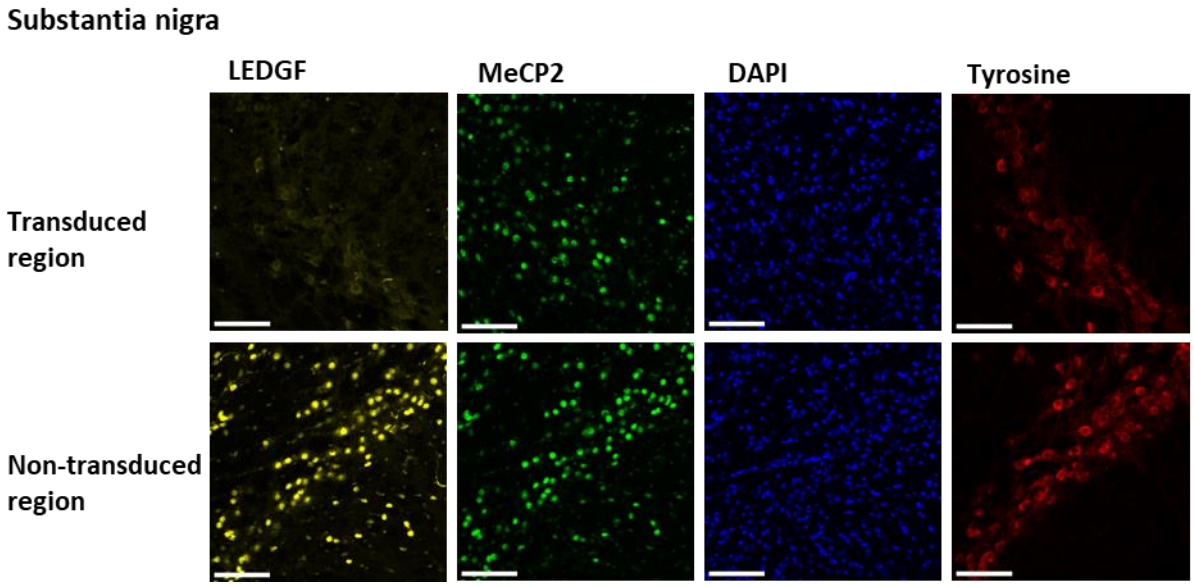

Figure 4.7: Validation of the *PSIP1* KO and effect on the MeCP2 protein levels in the substantia nigra. Brain slices of the transduced region and non-transduced region are shown. Antigen retrieval with citrate buffer was performed prior to incubation with the monoclonal mouse anti-LEDGF antibody, which stains both LEDGF isoforms. Fluorochrome-conjugated anti-mouse Alexa 555 IgG was used as a secondary antibody. The brain slices were stained with the polyclonal rabbit anti-MeCP2 antibody and the fluorochrome-conjugated anti-rabbit Alexa 488 IgG was used as a secondary antibody. The nuclear DAPI staining and the polyclonal chicken anti-TH antibody with the fluorochrome-conjugated anti-chicken Alexa 633 IgG secondary antibody were additionally used. Slices were mounted with a cover slip and Mowiol. Pictures were taken with the confocal microscope. Magnification = 20X. The scale bar = 100 µm.

The pictures were quantified to determine the protein expression. LEDGF and MeCP2 are nuclear proteins. Therefore, the mean pixel intensity per nucleus was measured for each ROI in the non-transduced and transduced regions. Figure 4.8 shows the effect of the Cre vector transduction on the mean LEDGF pixel intensity per nucleus in the different brain regions across the biological duplicates or triplicates.

The mean LEDGF pixel intensity per nucleus was quantified in the non-transduced and transduced region. The baseline values of the non-transduced region differ between biological duplicates and among different brain regions. After transduction, the residual mean pixel intensity per nucleus of LEDGF was strongly decreased. The ratio, shown in Figure 4.9, was taken to control for the variability between mice. The striatum was identified as the region where the greatest decrease of mean LEDGF pixel intensity per nucleus was observed (95%). A five-fold decrease in LEDGF signal was obtained in the hippocampus and cortex. The residual LEDGF expression in the dopaminergic regions was 33-34% of the baseline signal. Additionally, as shown in Table 4.3 the dopaminergic regions had a decrease in LEDGF signal from more than 60%. Moreover, the cortex of mouse 1, the VTA and SN are the brain regions where the highest residual LEDGF levels were obtained (Figures 4.8B, D and E). As can be seen in Figure 4.8, the baseline mean pixel intensity per nucleus is higher in the striatum and cortex of

mouse 1 compared to the signal in the hippocampus. In the non-transduced dopaminergic regions, the mean pixel intensity per nucleus fluctuated around an intensity of 10 to 20.

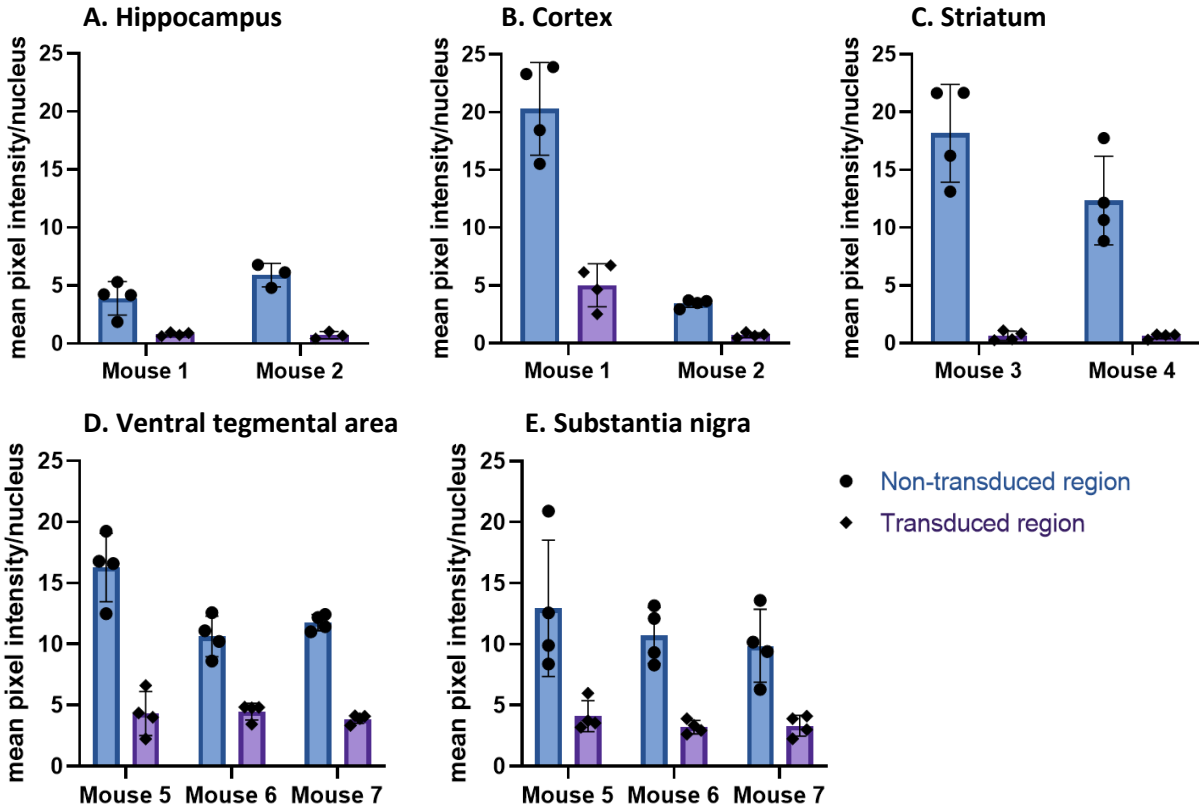

Figure 4.8: The mean LEDGF/p75 and LEDGF/p52 pixel intensity per nucleus measured for different brain regions in the non-transduced and transduced region. The mean LEDGF/p75 and LEDGF/p52 pixel intensity per nucleus was compared between the transduced and non-transduced regions. The analysis was performed in biological duplicates or triplicates. Each effect in a biological replicate is derived from technical quadruplicates. However, the data from the hippocampus in mouse 2 is derived from technical triplicates. The LEDGF/p75 and LEDGF/p52 protein levels in different brain regions were quantified as mean pixel intensity per nucleus and the error bars represent the standard deviation. The graph shows the baseline and residual LEDGF levels in **A.** hippocampus, **B.** Cortex, **C.** Striatum, **D.** Ventral tegmental area and **E.** Substantia nigra.

Table 4.3: Ratio and percentage reduction of LEDGF signal in the transduced region.

Brain region	Ratio [SD]	LEDGF signal reduction (%) [SD]
Hippocampus	0.1737 [+- 0.079]	82.63 [+- 7.90]
Cortex	0.2277 [+- 0.027]	77.23 [+- 2.72]
Striatum	0.0466 [+- 0.009]	95.34 [+- 0.91]
Ventral tegmental area	0.3428 [+- 0.081]	65.72 [+- 8.12]
Substantia nigra	0.3306 [+- 0.023]	66.94 [+- 2.37]

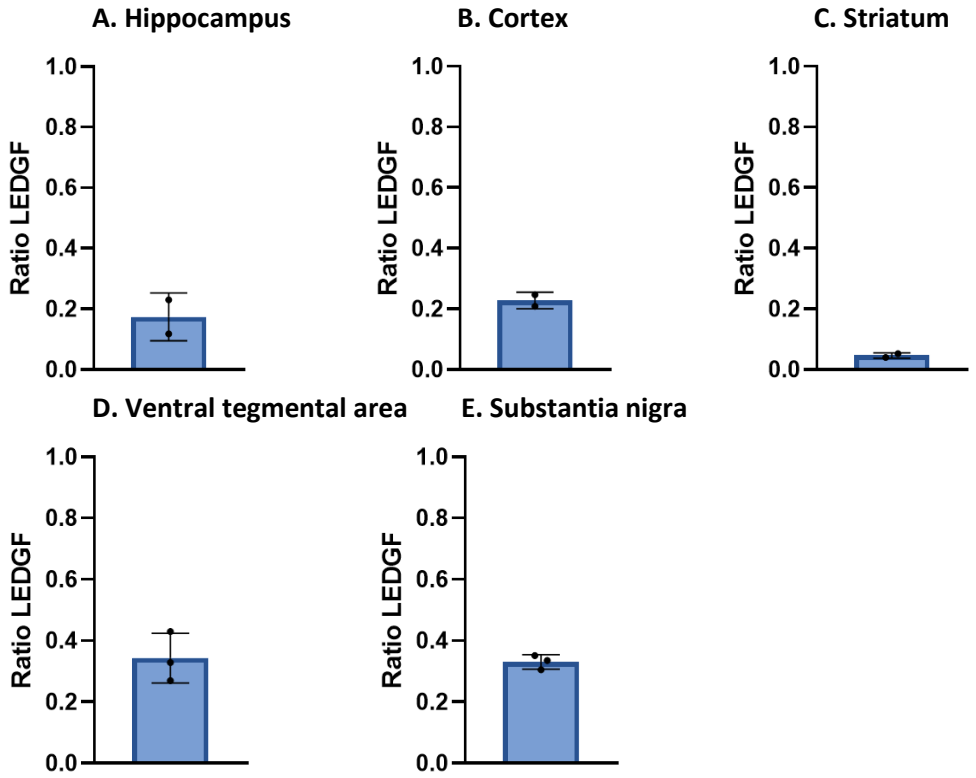

Figure 4.9: Ratio taken from the mean pixel intensity per nucleus of LEDGF in the transduced region over mean pixel intensity per nucleus of LEDGF in the non-transduced region. The ratio was taken for every ROI **A.** Hippocampus, **B.** Cortex, **C.** Striatum, **D.** Ventral tegmental area and **E.** Substantia nigra. The error bars represent the standard deviation.

4.2.4 Neurotoxicity of the Cre vector

To control that the observed reduction in mean LEDGF pixel intensity per nucleus is due to a *PSIP1* KO, a control experiment was performed. A double staining with the anti-NeuN and anti-Cre antibody was performed to determine if the transduction induced neurotoxicity. After visual inspection of every ROI via fluorescent microscopy (Figure 4.5) and visual analysis of the hippocampus and cortex via confocal microscopy (Figure 4.10), no neurotoxicity was observed. Furthermore, the number of neurons in the hippocampus and cortex were quantified via neuronal staining with the anti-NeuN antibody. Confocal pictures of the non-transduced and transduced region were taken. As can be seen in Figure 4.10, the number of neurons per µm² do not differ between the non-transduced and transduced region. Furthermore, there were less cells/µm² in the cortex compared to the hippocampus.

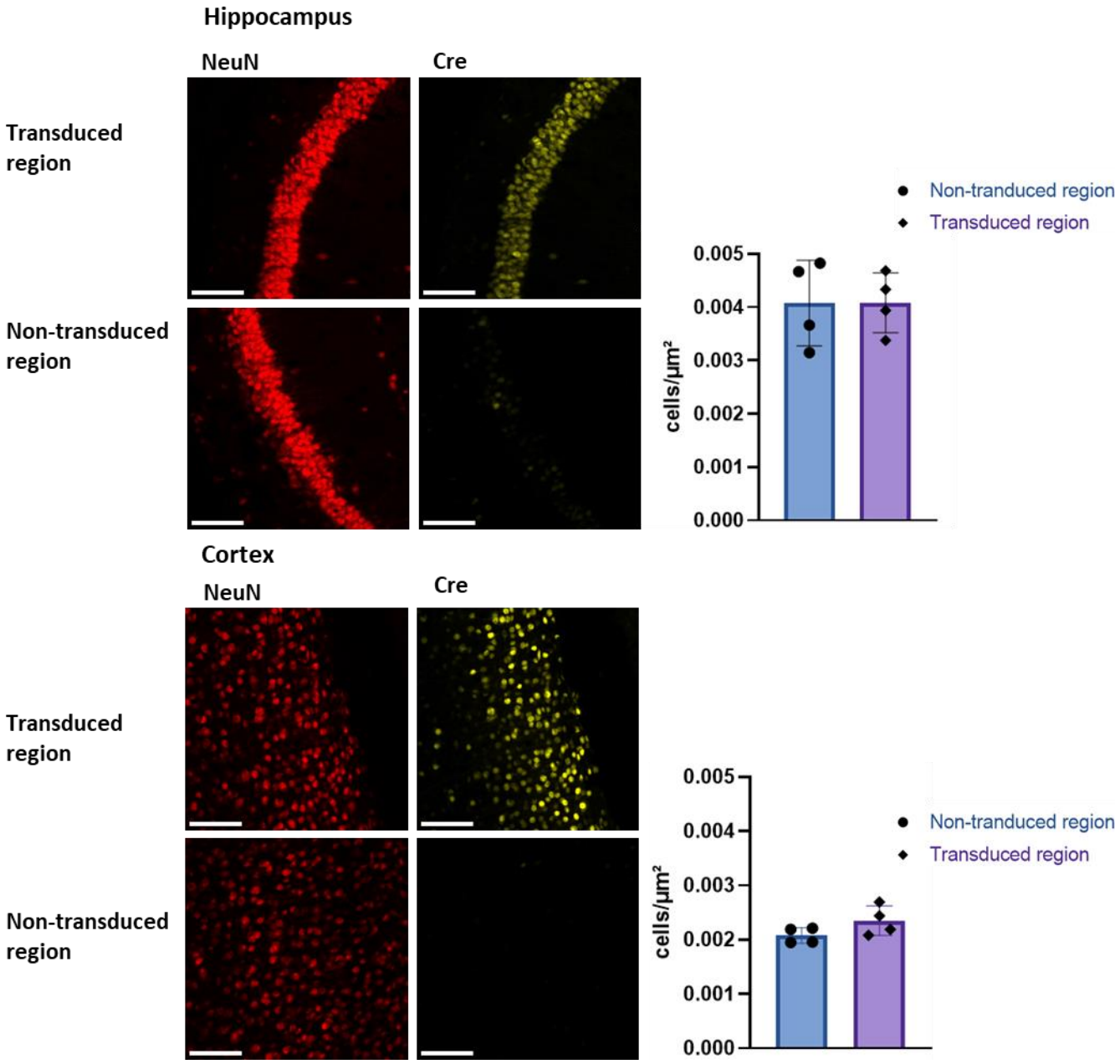

Figure 4.10: Validation of the Cre vector induced neurotoxicity. Antigen retrieval with citrate buffer was performed. The hippocampus was stained with the primary polyclonal chicken anti-NeuN antibody and the secondary fluorochrome-conjugated goat anti-chicken Alexa 633 IgG to indicate the neurons. Staining for the primary monoclonal mouse anti-Cre antibody and the secondary fluorochrome-conjugated goat anti-mouse Alexa 555 IgG antibody was additionally accomplished to discriminate the transduced region from the non-transduced region. The slices were covered with a cover slip and Mowiol. The pictures were taken with a confocal microscope. Magnification = 20X. The scale bar = 100 µm. Quantification of the number of cells/µm² in the non-transduced and transduced region of the hippocampus and cortex. The error bars represent the standard deviation.

4.2.5 Quantification of MeCP2 protein levels in the *PSIP1* knock-out region

To accomplish the second objective, the influence on the MeCP2 protein levels in different *PSIP1* KO brain regions was determined after validating the locally induced *PSIP1* KO.

The MeCP2 staining is shown in Figures 4.6 and 4.7. The pictures were quantified with QuPath to determine the difference in protein expression in the transduced region compared to the MeCP2 protein expression in the non-transduced region. Because MeCP2 is a nuclear protein, the pixel intensity in the nucleus was measured. The images were captured using a confocal microscope.

As shown in Figures 4.11A, B and E, the MeCP2 levels decreased in the transduced region compared to the non-transduced region. This applies to the brain regions such as the hippocampus, cortex and the SN. The mean MeCP2 pixel intensity per nucleus was decreased in two of the three VTAs (Figure 4.11D). However, mouse 6 has no alteration in the mean MeCP2 pixel intensity per nucleus. Moreover, the mean MeCP2 pixel intensity per nucleus in the striatum differs between the biological duplicates. Figure 4.11C shows that mouse 3 has a decrease in the mean MeCP2 pixel intensity per nucleus after transduction with the Cre vector. On the contrary, mouse 4 has a slight increase in the mean MeCP2 pixel intensity per nucleus in the transduced region. The baseline mean MeCP2 intensity levels in the hippocampus, striatum and in the cortex of mouse 2 were situated around a value of 10. The SN and VTA has comparable values for the mean pixel intensity per nucleus in the non-transduced region.

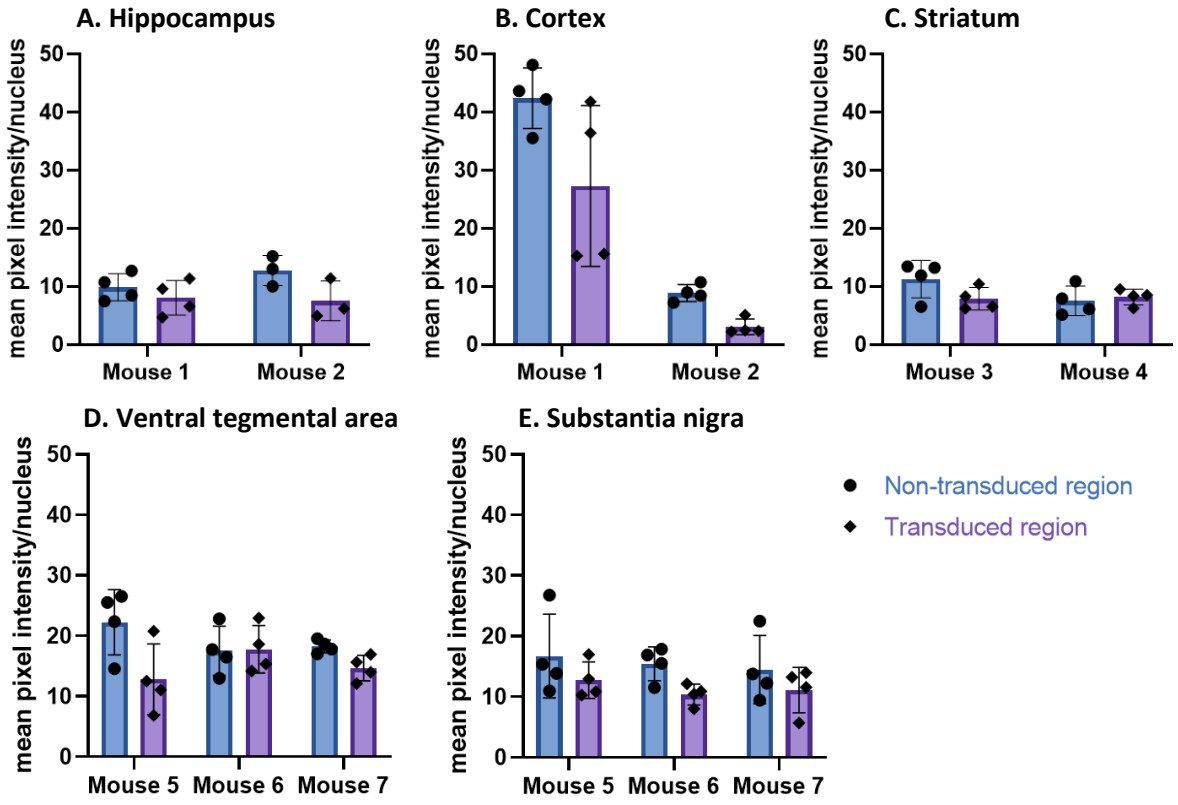

Figure 4.11: The measured mean MeCP2 pixel intensity per nucleus for different brain regions in the non-transduced and transduced region. A. The mean MeCP2 pixel intensity per nucleus is shown for the non-transduced and transduced regions in the hippocampus for the two biological replicates. The effect obtained in a biological replicate is derived from four technical replicates. However, the data from the hippocampus in mouse 2 is derived from technical triplicates. **B.** Cortex, **C.** Striatum, **D.** Ventral tegmental area and **E.** Substantia nigra. The error bars represent the standard deviation.

For every ROI, the ratio was taken for each biological replicate to correct for the variability between mice. The ratio was calculated by dividing the mean pixel intensity per nucleus of MeCP2 in the transduced region by the mean MeCP2 pixel intensity per nucleus in the non-transduced region.

As shown in Figures 4.12A, B and E, the ratio of the mean MECP2 pixel intensity per nucleus in the hippocampus, cortex and SN are smaller than one. This means that the MeCP2 mean pixel intensity per nucleus in the transduced region was lower than the MeCP2 mean pixel intensity per nucleus in the non-transduced region. For example, as shown in Figure 4.12A, the obtained ratio in the hippocampus was 0.7. This means that the MeCP2 signal in the transduced site is 0.7 times the signal obtained in the non-transduced site. In addition to these results, Table 4.4 provides the percentage of reduction of the MeCP2 signal. According to the previous example of the hippocampus, a reduction from 30% is obtained in the transduced site compared with the non-transduced site.

As shown in Figure 4.12B and Table 4.4, the strongest reduction (49%) between the different brain regions, was obtained in the cortex. Furthermore, the MeCP2 ratio was lower than one in the VTA. However, taking the standard deviation into account, the range of the ratio was bigger than one. The ratio of the VTA is shown in Figure 4.12D. The MeCP2 ratio of the striatum is equal to one and is presented in Figure 4.12C. As shown in Table 4.4, a negligible reduction of 1% was obtained in the striatum.

Table 4.4: Ratio and percentage reduction of MeCP2 signal in the transduced region.

Brain region	Ratio [SD]	MeCP2 signal reduction (%) [SD]
Hippocampus	0.70 [+- 0.18]	29.65 [+- 18.33]
Cortex	0.51 [+- 0.22]	48.58 [+- 22.62]
Striatum	0.99 [+- 0.25]	1.10 [+- 24.88]
Ventral tegmental area	0.83 [+- 0.24]	17.42 [+- 23.84]
Substantia nigra	0.78 [+- 0.07]	22.15 [+- 7.19]

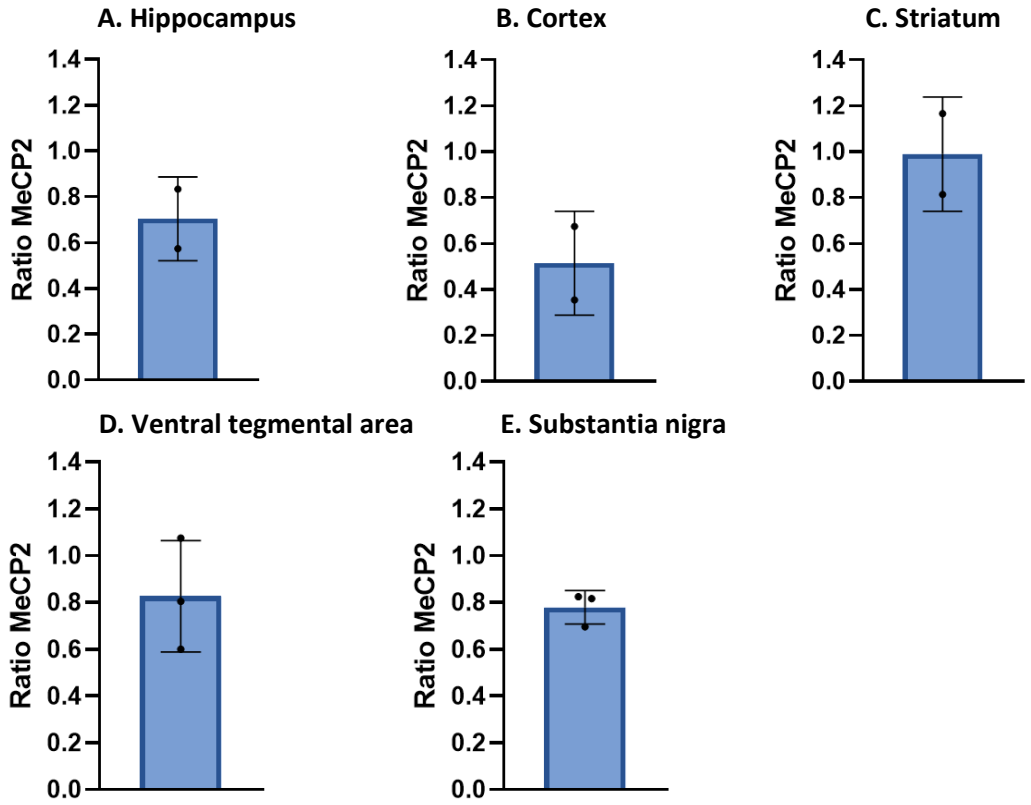

Figure 4.12: Ratio taken from the mean pixel intensity per nucleus of MeCP2 in the transduced region over mean pixel intensity per nucleus of MeCP2 in the non-transduced region. The ratio was taken for every ROI **A.** Hippocampus, **B.** Cortex, **C.** Striatum, **D.** Ventral tegmental area and **E.** Substantia nigra. The error bars represent the standard deviation.

5 DISCUSSION

5.1 LOCAL KNOCK-OUT OF MECP2 OR LEDGF IN HEK293T CELLS

The first research aim was to validate the designed DNA constructs for their capabilities to KO the *PSIP1* gene or *MeCP2* gene. Afterwards, the most potent DNA construct to KO the *PSIP1* gene or the *MeCP2* gene was chosen. The second aim was to validate the created *PSIP1* KO cell line and the *MeCP2* KO cell line.

The results in this master thesis underscore the important role of validating the potential of the DNA constructs for their ability to create indels. The transfection efficiency between the technical replicates differed according to the percentage of EGFP positive cells in the flow cytometry analysis. In the study of Rahimi et al., the transfection efficiency of an EGFP plasmid performed with Lipofectamine 3000 in HEK293T cells was 52% (91). Both performed transfection experiments shown in Figure 4.1, have a higher percentage of EGFP-positive cells (78% and 62%) than in the study performed by Rahmini et al. However, not each transfected cell created a mutation, as can be seen in Figure 4.1 and Table 4.1. Especially in the second transfection experiment, the quantity of frameshift mutations was extremely low (1-9%), while the transfection efficiency did not show such a low efficiency. In a study performed by Liang et al. HEK293T cells were transfected with a Cas9 plasmid using Lipofectamine 3000. In this research, 49% of the transfected HEK293T cells created an indel (92). In comparison, the results of both transfection experiments listed in Table 4.1, did not reach the indel percentage of 49%. A discrepancy between the transfection efficiency and the percentage of created indels occurred. Our data shows that the transfection efficiency in HEK293T cells was higher than the reported 49-52%. However, the used DNA constructs were not able to create mutations in every transfected cell.

After the validation of the DNA constructs, the most potential DNA construct was chosen to create the KO cell line using VLPs. The determination of the KO was performed on the DNA, RNA and protein level.

The *PSIP1* KO HEK293T cell line was successfully created. The sequencing of the *PSIP1* KO polyclonal cell line revealed that in 96% of the cells an indel was created. Unlike the research of Mangeot et al., which also used murine leukemia virus-based VLPs to edit human-induced pluripotent cells, where 67% of the cell were modified (85). As shown in Figures 4.3D and E, the RT-qPCR data indicate that the residual RNA for both LEDGF isoforms was very low. The residual protein levels of LEDGF/p75 and LEDGF/p52 were not detectable anymore on a Western blot. Similarly, the quantification of the Western blot did not reveal any residual LEDGF protein levels (Figures 4.3B and C). Therefore, the influence of the remaining RNA and protein levels in the polyclonal *PSIP1* KO cell line is expected to be low.

In contrast to the *PSIP1* KO cell line, the DNA construct for MeCP2 was not sufficient to KO the *MeCP2* gene. According to the results shown in Figure 4.2C, the residual MeCP2 RNA levels were still high (67%). In addition, the MeCP2 protein is slightly visible on the Western blot. Remarkably, the data of the Western blot, shown in Figures 4.2A and B, indicates a reduction of the MeCP2 protein in the *MeCP2* KO cell line which is not the case for the RNA levels.

Initial observations in the Western blot and quantification data suggest that there is an effect of the *PSIP1* KO on the MeCP2 protein levels (Figures 4.2A and B) in HEK293T cells. Moreover, this experiment studied also the reverse situation (Figures 4.3A-C). Remarkably, the LEDGF/p75 and LEDGF/p52 protein levels were decreased in a *MeCP2* KO cell. These data indicate that LEDGF and MeCP2 interfere with each other's expression pattern. In the reported quantification (Figures 4.2B and 4.3B and C), the protein levels were normalised to vinculin. The obtained decrease of MeCP2 or LEDGF protein levels is not due to variability in loading. In the past, different LEDGF knock-down cell lines were analysed to find an effect on MeCP2 levels. However, no conclusive effect was obtained.

5.1.1 Limitations and strengths

Lipofectamine 3000, which is used in the transfection experiments, is a useful transfection reagent to transfect HEK293T cells. According to research by Rahimi et al. and Liang et al., Lipofectamine 3000 transfected adherent cells such as HEK293T cells, with plasmids in an efficient way (91, 92).

It is challenging to package sgRNAs in VLPs. A sgRNA is stable in a VLP when it is complexed with a Cas9 enzyme (93). This hurdle is bridged in the production of VLPs by the Leuven Viral Vector Core. Furthermore, an advantage of creating a KO cell line via transducing the cells with those VLPs is that the KO cell line is polyclonal. A monoclonal cell line has no longer to be produced, which saves resources, cost and time. The extra advantage of using a polyclonal cell line is that the effect is studied in a genetically divers cell population, which enhance the robustness of the observed effects.

An important note to make is that during the second transfection experiment, the cells were not to the same degree single cells as in the first transfection experiment. This has implications for the analysis with the flow cytometry because only single EGFP positive cells can be gated. This can explain why the second transfection efficiency is lower. However, the lower transfection efficiency does not fully explain why in the second experiment the cells did not create much mutations.

One major drawback of the transduction process is that the transduction efficiency was not measured in the production of the KO cell lines. However, research by Mangeot et al. measured a transduction efficiency of 100% after 16h (85). The HEK293T cell lines, in the reported experiments, were transduced with the VLPs for more than 16h. It is likely that all the cells were transduced. However, not every cell

had a KO of the gene of interest. This phenomenon might arise because the sgRNA, generated from the DNA construct, was inadequate to fully KO the gene of interest.

The interpretation of the results depends on the used analysis tool. The output of each analysis tool was slightly different and the reconstruction of the percentage of the created mutations varies between the two tools. Decodr had more issues with reading the raw sequencing data which led to less reconstructed results. A trend that is visible as well, is that the percentage of frameshift mutations was consistently higher in the performed reconstruction by Decodr compared with the percentage of created indels and the KO-score provided by ICE. Therefore, it is important to critically compare the analysing programs with each other. Specifically, Decodr is more able to analyse different features of the mutations. For example, Decodr surpasses ICE in analysing large deletions (>100 bp) and it also outperforms ICE in analysing insertions (84). However, it is worth noting that insertions were not the main mutation in the KO cell lines.

Finally, the Western blot is performed in HEK293T cells. Using these cells has the advantage of working in a human derived *in vitro* model. Furthermore, these findings also suggest an effect of MeCP2 on LEDGF. It is important to note that this experiment is performed once. Future experiments have to be performed to find out if this is a recurring obtained effect. In the second part of this master's thesis an effect between LEDGF on MeCP2 is sought in different mouse brain regions. The results from the HEK293T cells have the benefit of indicating that the impact of LEDGF on MeCP2 also occurs in human cells.

5.1.2 Future prospects

RNA-sequencing can be performed on the *PSIP1* KO cell line. The RNA-sequencing results can determine which genes are downregulated in a *PSIP1* KO cell line. However, to address the research question, the *PSIP1* KO as well as the *MeCP2* KO cell line have to be analysed to determine the subset of genes which are affected by the MeCP2-LEDGF protein complex. However, the production of a full *MeCP2* KO was not successful. A second transduction of the cell line with the VLPs could create more mutations and KO the residual *MeCP2* gene. In the future, a successful *MeCP2* KO cell line could be used to measure the change in LEDGF/p75 and LEDGF/p52 expression in a MeCP2 protein-depleted cell.

Further studies are necessary to determine how large the effect of the *PSIP1* or *MeCP2* KO is on the MECP2 or LEDGF protein levels. These results can provide more insight into the formation of the MeCP2-LEDGF protein complex. Similarly, Western blots from HEK293T derived protein samples can also be stained with the anti-ORF1p antibody. These experiments will shed a light on the LINE-1 derived proteins in a KO cell. The amount of ORF1p indicates the translation of mRNA into proteins. ORF1p and

ORF2p are necessary elements in the LINE-1 retrotransposition process. However, measuring of the retrotransposition activity of LINE-1 elements can also be done by performing a LINE-1 retrotransposition assay.

The RT-qPCR data were normalised to GAPDH in contrast to the Western blot data, which was normalised to vinculin. In the future, the Western blot can also be stained for GAPDH as housekeeping protein. In this way the quantification of the protein levels in the Western blot is normalised to the same protein as in the RT-qPCR data. This results in more translational data to compare the RNA levels with the protein levels. However, practical feasibility is not great. GAPDH is a protein with a weight of 37 kDa that runs closely to LEDGF/p52, with a weight of 52 kDa. The blot has to be cut around 40 kDa, which can damage the blot and proteins, in order to incubate the blots simultaneously with the primary anti-GAPDH or anti-LEDGF/p52 antibody.

To conclude, the designed DNA constructs can create mutations in cells to KO the gene of interest. The transduction of the HEK293T cells with the VLPs revealed that the DNA constructs were not potent enough to KO the gene of interest in each cell completely. However, the DNA construct to KO the *PSIP1* gene is more potent than the DNA construct to KO the *MeCP2* gene. Therefore, the transduction with the VLPs to KO the *PSIP1* gene was successful. Nevertheless, the KO of the *MeCP2* gene is not complete. There are still residual MeCP2 RNA levels and the proteins come partially to expression.

5.2 LOCAL *IN VIVO* KNOCK-OUT OF LEDGF

The scope of the performed experiments was to validate the created *PSIP1* KO and to find a possible tendency in the MeCP2 protein levels in the locally induced *PSIP1* KO brain region. A pilot study was set up to address this research question. Because the number of biological replicates is two or three, the sample size was too small to create significant differences. Due to this reason, no statistical tests are performed on the results.

First of all, *PSIP1*$^{fl/fl}$ C57BL/6J mice had to be identified. The mice which have a DNA band at 802 bp were identified as *PSIP1*$^{fl/fl}$ C57BL/6J mice. In contrast to the height of a *PSIP1*$^{fl/fl}$ DNA band, the DNA band of a *PSIP1*$^{WT/WT}$ mouse is located at a height of 745 bp. The difference in length of the *PSIP1 gene* is only 57 bp. Therefore, the difference is not always easily visible on an agarose gel. Furthermore, the *PSIP1*$^{fl/fl}$ has to be homozygous, when a band on 802 and 745 bp appears the mouse was classified as heterozygous and not selected for further usage.

The validation of the *PSIP1* KO consists of two research aims: the validation of the transduction with the Cre vector and the effect of the transduction on the LEDGF protein levels. First, the Cre vector

transduced every cell type in the ROI. However, the Cre enzyme came only to expression in neurons because the synapsin-promoter is a neuron-specific promoter. The non-transduced and transduced region were validated via the staining of the Cre enzyme. The Cre enzyme levels in the transduced region were strongly visible (Figure 4.5 and 4.10). Thus, the stereotactic injection targeted every ROI and the cells are efficiently transduced with the vector. Subsequently, the number of cells/µm² was similar in the non-transduced and transduced regions (Figure 4.10). Therefore, the conclusion was made that the transduction of the ROI did not induce local neurotoxicity. Royo et al., studied the toxicity of different AAV serotypes in the hippocampus and cortex (94). In accordance with our data, the study shows that the transduction with a AAV-serotype 2 did not induce neurotoxicity (94). In addition, the obtained reduction in protein levels, shown in Figures 4.8 and 4.11, were certainly not achieved via a loss of neurons in the transduced region.

2 µL of a $5*10^9$ GC/mL viral vector solution was injected into each brain regions. However, the Cre vector did not spread in a similar way between biological replicates. The concentration and volume was previously optimised for injections in the SN. To achieve more viral vector spreading through the ROI, using different injection volumes and concentrations can help to achieve better spreading because spreading of the vector depends on the injected concentration but also on the volume. Different concentrations and volumes are reported in literature. Scheyltjens et al. reported a comprehensive spreading of a rAAV2/7-CMV-intron-eGFP using 0.2 µL containing $1.90*10^{12}$ GC/mL (82). A prior study by Van der Perren et al., reported a successful spreading of rAAV2/7 in a mouse's hippocampus using 3 µL of a viral vector solution of $1.0*10^{10}$ GC/mL (83). It is not likely that increasing the viral vector concentration induces neurotoxicity. Royo et al. found no neurotoxicity in cultured neurons using 0.2 µL of $2.0\text{-}2.5*10^{11}$ GC/mL of AAV2 (94).

Secondly, via the determination of the LEDGF/p75 and LEDGF/p52 protein levels, the influence of the transduction with the Cre vector to KO the *PSIP1* gene in neurons was studied. As can be seen in Figure 4.5, the Cre vector was able to KO the *PSIP1* gene and reduce the protein levels *in vivo*. Moreover, Figures 4.8 and 4.9 show that every ROI was susceptible to create a *PSIP1* KO with the viral vector because the mean LEDGF pixel intensity per nucleus was decreased in the transduced region compared to the non-transduced region. The biological replicates had different baseline levels of mean LEDGF pixel intensity per nucleus. In contrast to the transduced regions, the residual mean LEDGF pixel intensity per nucleus was almost equal between the biological replicates. However, these finding were not applicable to the cortex. The phenomena of equal residual obtained signals could provide evidence that all neurons were targeted. The residual signal could be derived from non-neuronal cells and background noise. According to the Brain RNA-seq database, LEDGF and MeCP2 are more prominently expressed in neurons. Residual, non-neuronal LEDGF or MeCP2 signal may result from expression in

oligodendrocytes, astrocytes, or endothelial cells. (95). Furthermore, the set threshold detection in QuPath was low in order to be able to detect all cells. However, it cannot be ruled out that some background noise is detected and quantified (Figure 4.8). As can be seen in Figure 4.7, there are still some LEDGF positive cells in the transduced region of the substantia nigra. The quantification with QuPath identified the cell nucleus, based on the MeCP2 staining. During the determination of the residual LEDGF signal, signal derived from non-neuronal cells were quantified as well. This phenomenon could partially explain the higher measured residual mean LEDGF/p75 and LEDGF/p52 pixel intensity per nucleus. To control for the variability between biological replicates, the ratio allows to compare the residual LEDGF levels between the ROIs. The ratio revealed that the LEDGF levels were reduced the most in the striatum and thereafter the hippocampus. A reduction of 77% was obtained in both biological replicates of the cortex. The residual mean LEDGF pixel intensity per nucleus was the highest in the dopaminergic regions. This can be the case since the fraction of oligodendrocytes and epithelial cells is higher in the SN and VTA compared to the hippocampus, striatum, and cortex (96).

The second scope of this master's thesis was to indicate the possible interaction between LEDGF and MeCP2. The influence of the *PSIP1* KO on the MeCP2 protein levels in different brain regions was studied. The MeCP2 signal was measured as mean pixel intensity per nucleus.

The influence of the *PSIP1* KO on the MeCP2 protein levels is an effect caused by the absence of both LEDGF isoforms. Despite a successful formed *PSIP1* KO, the MeCP2 levels did not always alter in every ROI (Figure 4.11). The decrease of MeCP2 protein levels in the transduced site was normalised to the basal MeCP2 protein expression to control for the variability between the biological replicates. The ratios are shown in Figure 4.12. When the ratio was lower than one, a consistent decrease among the biological replicates occurred. In three out of the five regions (hippocampus, cortex and SN) the MeCP2 levels decreased in every biological replicate. The strongest reduction occurred in the cortex. However, the reduction with the less variability between the mice was obtained in the SN. Besides, the MeCP2 levels in the VTA decreased in two of the three biological replicates. Furthermore, the highest reduction in LEDGF proteins were obtained in the striatum. However, no consistent effect of the *PSIP1* KO was observed.

Olson et al., studied the protein levels of the distinct MeCP2 isoforms in different adult mouse brain regions (52). This research reported a constant E1 MeCP2 level throughout different brain regions such as hippocampus, cortex and striatum. The protein levels of the E2 isoform differed between those regions. The MeCP2 E2 levels were comparable between the striatum and the hippocampus and the E2 levels are lower in the cortex (52). In this master's thesis, the antibody stained both isoforms. The baseline MeCP2 levels in the hippocampus and striatum are similar (Figure 4.11A and C). The

MeCP2 baseline levels in the cortex of mouse 2 are comparable with the MeCP2 levels in the hippocampus and striatum. However, the MeCP2 levels of mouse 1, in the non-transduced region of the cortex were 4 times higher. Wither et al., studied the effect of reduced MeCP2 levels in a $MeCP2^{+/-}$ mouse model. This research reported that the MeCP2 expression was not uniform reduced in the same brain region among 10 $MeCP2^{+/-}$ mice. The expression was measured in the hippocampus and cortex (97). Even though the small sample size, this event is also obtained in the reported data in Figure 4.11.

5.2.1 Limitations and strengths

Performing the genotyping via ear punches has multiple advantages. First of all, the ear biopsy is an operation which induces minimal distress or pain. Subsequently, taking ear punches will mark the mice and make identifying the mice easier. At last, no anaesthesia or analgesia are required to take this type of biopsies (98, 99).

The anti LEDGF/p75 antibody used in the validation of the Cre vector injections (Figure 4.5) only stained the LEDGF/p75 isoform. Therefore, in the validation of the PSIP1 KO in the transduced regions (Figures 4.6 and 4.7), the anti LEDGF antibody, which stains both isoforms, is used. In this way, a more global idea of the PSIP1 KO on the overall LEDGF/p75 and LEDGF/p52 protein levels was achieved.

The possibility to induce a regional *PSIP1* KO in a mouse brain is a useful model to study the role of LEDGF in each brain region separately. This mouse model can provide more insight in the role of LEDGF in different brain regions to explain observed phenotypic characteristics, which are explored in a conditional mouse model. Furthermore, the postnatally induced *PSIP1* KO can help to distinguish if the observed effects are due to developmental shortage of LEDGF or post-developmental induced deficits. An extra advantage of this *in vivo PSIP1* KO mouse model is to analyse the selective depletion of LEDGF in neurons. This is in contrast to the conditional *PSIP1* KO mouse model, which has a *PSIP1* KO in neural stem cells. These neural stem cells differentiate into neurons, astrocytes and oligodendrocytes (100).

The mouse brain is preferentially sliced with the vibratome in slices of 40 µm. However, due to technical limitations the thickness of slices can diverge. Moreover, the used gelatine-coated slices are made in-house. A limitation of these slices is that the regional thickness of the gelatine layer can fluctuate. All these findings are notable under the confocal microscope. For every picture that was taken with the confocal microscope, the picture was visually adjusted on the DAPI staining to achieve the same focus between technical replicates. However, variability in focus between pictures cannot be excluded.

An artifact in the cortex of mouse 2 occurred. We assume that this artifact can partially explain why the obtained differences in the absolute LEDGF and MeCP2 expression between biological replicates were so high. This artifact could be induced by neurotoxicity, the stereotactic injections or an unknown

phenomenon of the induced *PSIP1* KO, which has to be further investigated. The artifact is not likely induced by the cutting or staining proses. The comparison between absolute values of the mean pixel intensity per nucleus is not feasible between the cortex and other brain regions. Therefore the ratio is taken to be able to compare these biological duplicates. The relative decrease is comparable between the ROI.

5.2.2 Future prospects

The research performed in this master thesis, indicates that an effect of the *PSIP1* KO on the MeCP2 levels is established in the hippocampus, cortex and SN. To generate a full picture of the impact of the *PSIP1* KO on the MeCP2 levels, additional studies will be needed. Consecutive research aims to analyze if other brain regions are susceptible for the alteration of MeCP2 levels after transduction with the Cre vector.

In successive research, the antibody anti-NeuN, which stains neuronal nuclei, can be added in order to detect especially the neurons to quantify the LEDGF and MeCP2 mean pixel intensities per nuclei. In this case, the signal is only obtained from neurons.

To develop a full picture of the possible Cre vector induced neurotoxicity, additional studies are needed. Besides a visual inspection for neurotoxicity, a quantification of the cells/µm² can additionally be performed on the striatum, VTA and SN. Those studies aim to confirm the non-neurotoxic effect of the Cre vector transductions in those regions.

In the future, this mouse model could serve as an *in vivo* model to study the role of LEDGF in specific brain regions. Further research can be performed to analyse if there are phenotypic influences of the KO on the targeted brain region. Additional work is needed to study whether the decrease in MeCP2 can result in RTT-like phenotypic behaviour in mice. In addition, one can study if the RTT-like phenotype is dependent on which brain region has a local MeCP2 decrease.

Moreover, additional experiments regarding the role of MeCP2 and LEDGF in LINE-1 retrotransposition would be worthwhile. Once the ORF1p-staining is optimised, the effect of the *PSIP1* KO on LINE-1 derived ORF1p can be examined.

To conclude, the Cre enzyme was expressed in all the ROIs. The transduction of the neurons with the Cre vector or expression of the Cre enzyme did not induce neurotoxicity. Therefore, the reduction in protein levels is not influenced by neuronal loss. In essence, the obtained, consistent LEDGF protein reduction in the transduced cells is due to the induced *PSIP1* KO. The locally induced *PSIP1* KO mouse model is validated and can be used in further experiments. The regionally induced *PSIP1* KO resulted in a decrease of MeCP2 proteins in certain brain regions such as the hippocampus, cortex and SN. These findings provide insights into the specific regional interaction between the possible regulators of LINE-1 retrotransposition in a mouse brain.

6 REFERENCES

1. Li R, Dong Q, Yuan X, Zeng X, Gao Y, Chiao C, et al. Misregulation of Alternative Splicing in a Mouse Model of Rett Syndrome. PLOS Genetics. 2016;12(6):e1006129.
2. McClintock B. The origin and behavior of mutable loci in maize. Proceedings of the National Academy of Sciences. 1950;36(6):344-55.
3. Biémont C, Vieira C. Junk DNA as an evolutionary force. Nature. 2006;443(7111):521-4.
4. Erwin JA, Marchetto MC, Gage FH. Mobile DNA elements in the generation of diversity and complexity in the brain. Nature Reviews Neuroscience. 2014;15(8):497-506.
5. Chuong EB, Elde NC, Feschotte C. Regulatory activities of transposable elements: from conflicts to benefits. Nature Reviews Genetics. 2017;18(2):71-86.
6. Richardson SR, Doucet AJ, Kopera HC, Moldovan JB, Garcia-Perez JL, Moran JV. The Influence of LINE-1 and SINE Retrotransposons on Mammalian Genomes. Microbiology Spectrum. 2015;3(2):1165-208.
7. Kazazian HH, Moran JV. Mobile DNA in Health and Disease. New England Journal of Medicine. 2017;377(4):361-70.
8. Suarez NA, Macia A, Muotri AR. LINE-1 retrotransposons in healthy and diseased human brain. Dev Neurobiol. 2018;78(5):434-55.
9. Encyclopaedia TEo. Eocene Epoch Encyclopedia Britannica: Britannica; 2013 [2022-11-08]. Available from: https://www.britannica.com/science/Eocene-Epoch.
10. Christensen T. HERVs in Neuropathogenesis. Journal of Neuroimmune Pharmacology. 2010;5(3):326-35.
11. Hashimoto K, Jouhilahti E-M, Töhönen V, Carninci P, Kere J, Katayama S. Embryonic LTR retrotransposons supply promoter modules to somatic tissues. Genome Research. 2021;31(11):1983-93.
12. Kim HS. Genomic impact, chromosomal distribution and transcriptional regulation of HERV elements. Mol Cells. 2012;33(6):539-44.
13. Grandi FC, An W. Non-LTR retrotransposons and microsatellites. Mobile Genetic Elements. 2013;3(4):e25674.
14. Ahmet, Narvaiza I, Bilal, Pena M, Benner C, Maria, et al. Primate-Specific ORF0 Contributes to Retrotransposon-Mediated Diversity. Cell. 2015;163(3):583-93.
15. Callahan KE, Hickman AB, Jones CE, Ghirlando R, Furano AV. Polymerization and nucleic acid-binding properties of human L1 ORF1 protein. Nucleic Acids Research. 2012;40(2):813-27.
16. Bodak M, Yu J, Ciaudo C. Regulation of LINE-1 in mammals. Biomolecular Concepts. 2014;5(5):409-28.
17. Hancks DC, Kazazian HH. Active human retrotransposons: variation and disease. Current Opinion in Genetics & Development. 2012;22(3):191-203.
18. Khazina E, Weichenrieder O. Human LINE-1 retrotransposition requires a metastable coiled coil and a positively charged N-terminus in L1ORF1p. eLife. 2018;7.
19. Naufer MN, Furano AV, Williams MC. Protein-nucleic acid interactions of LINE-1 ORF1p. Semin Cell Dev Biol. 2019;86:140-9.
20. Zhang X, Zhang R, Yu J. New Understanding of the Relevant Role of LINE-1 Retrotransposition in Human Disease and Immune Modulation. Front Cell Dev Biol. 2020;8:657.
21. Honda T, Nishikawa Y, Nishimura K, Teng D, Takemoto K, Ueda K. Effects of activation of the LINE-1 antisense promoter on the growth of cultured cells. Scientific Reports. 2020;10(1).
22. Martin MD, Brown DN, Ramos KS. Computational modeling of RNase, antisense ORF0 RNA, and intracellular compartmentation and their impact on the life cycle of the line retrotransposon. Comput Struct Biotechnol J. 2021;19:5667-77.
23. Bernardi R, Papa A, Pandolfi PP. Regulation of apoptosis by PML and the PML-NBs. Oncogene. 2008;27(48):6299-312.
24. Murat P, Balasubramanian S. Existence and consequences of G-quadruplex structures in DNA. Current Opinion in Genetics & Development. 2014;25:22-9.

25. Piskareva O, Schmatchenko V. DNA polymerization by the reverse transcriptase of the human L1 retrotransposon on its own template in vitro. FEBS Lett. 2006;580(2):661-8.
26. Lexa M, Steflova P, Martinek T, Vorlickova M, Vyskot B, Kejnovsky E. Guanine quadruplexes are formed by specific regions of human transposable elements. BMC Genomics. 2014;15(1):1032.
27. Sokolowski M, Deharo D, Christian CM, Kines KJ, Belancio VP. Characterization of L1 ORF1p Self-Interaction and Cellular Localization Using a Mammalian Two-Hybrid System. PLoS ONE. 2013;8(12):e82021.
28. Kulpa DA, Moran JV. Cis-preferential LINE-1 reverse transcriptase activity in ribonucleoprotein particles. Nat Struct Mol Biol. 2006;13(7):655-60.
29. Gorbunova V, Seluanov A, Mita P, McKerrow W, Fenyö D, Boeke JD, et al. The role of retrotransposable elements in ageing and age-associated diseases. Nature. 2021;596(7870):43-53.
30. Wei W, Gilbert N, Ooi SL, Lawler JF, Ostertag EM, Kazazian HH, et al. Human L1 Retrotransposition: cis Preference versus trans Complementation. Molecular and Cellular Biology. 2001;21(4):1429-39.
31. Taylor MS, Altukhov I, Molloy KR, Mita P, Jiang H, Adney EM, et al. Dissection of affinity captured LINE-1 macromolecular complexes. Elife. 2018;7.
32. Peze-Heidsieck E, Bonnifet T, Znaidi R, Ravel-Godreuil C, Massiani-Beaudoin O, Joshi RL, et al. Retrotransposons as a Source of DNA Damage in Neurodegeneration. Front Aging Neurosci. 2021;13:786897.
33. Bachiller S, Del-Pozo-Martín Y, Carrión Á M. L1 retrotransposition alters the hippocampal genomic landscape enabling memory formation. Brain Behav Immun. 2017;64:65-70.
34. Richardson SR, Morell S, Faulkner GJ. L1 Retrotransposons and Somatic Mosaicism in the Brain. Annual Review of Genetics. 2014;48(1):1-27.
35. Muotri AR, Zhao C, Marchetto MCN, Gage FH. Environmental influence on L1 retrotransposons in the adult hippocampus. Hippocampus. 2009;19(10):1002-7.
36. Li W, Prazak L, Chatterjee N, Grüninger S, Krug L, Theodorou D, et al. Activation of transposable elements during aging and neuronal decline in Drosophila. Nature Neuroscience. 2013;16(5):529-31.
37. Muotri AR, Marchetto MCN, Coufal NG, Oefner R, Yeo G, Nakashima K, et al. L1 retrotransposition in neurons is modulated by MeCP2. Nature. 2010;468(7322):443-6.
38. Nan X, Ng H-H, Johnson CA, Laherty CD, Turner BM, Eisenman RN, et al. Transcriptional repression by the methyl-CpG-binding protein MeCP2 involves a histone deacetylase complex. Nature. 1998;393(6683):386-9.
39. Liyanage VRB, Olson CO, Zachariah RM, Davie JR, Rastegar M. DNA Methylation Contributes to the Differential Expression Levels of Mecp2 in Male Mice Neurons and Astrocytes. International Journal of Molecular Sciences. 2019;20(8):1845.
40. Rodrigues DC, Mufteev M, Ellis J. Regulation, diversity and function of MECP2 exon and 3'UTR isoforms. Hum Mol Genet. 2020;29(R1):R89-r99.
41. Schmidt A, Zhang H, Cardoso MC. MeCP2 and Chromatin Compartmentalization. Cells. 2020;9(4):878.
42. Sharifi O, Yasui DH. The Molecular Functions of MeCP2 in Rett Syndrome Pathology. Front Genet. 2021;12:624290.
43. Good KV, Vincent JB, Ausió J. MeCP2: The Genetic Driver of Rett Syndrome Epigenetics. Front Genet. 2021;12:620859.
44. Mushtaq AU, Lee Y, Hwang E, Bang JK, Hong E, Byun Y, et al. Biophysical characterization of the basic cluster in the transcription repression domain of human MeCP2 with AT-rich DNA. Biochem Biophys Res Commun. 2018;495(1):145-50.
45. Martínez De Paz A, Khajavi L, Martin H, Claveria-Gimeno R, Tom Dieck S, Cheema MS, et al. MeCP2-E1 isoform is a dynamically expressed, weakly DNA-bound protein with different protein and DNA interactions compared to MeCP2-E2. Epigenetics & Chromatin. 2019;12(1).

46. Filarsky M, Zillner K, Araya I, Villar-Garea A, Merkl R, Längst G, et al. The extended AT-hook is a novel RNA binding motif. RNA Biology. 2015;12(8):864-76.
47. Steven, Chen L, Angela, Yu P, Lichtarge O, Huda. An AT-Hook Domain in MeCP2 Determines the Clinical Course of Rett Syndrome and Related Disorders. Cell. 2013;152(5):984-96.
48. Pejhan S, Rastegar M. Role of DNA Methyl-CpG-Binding Protein MeCP2 in Rett Syndrome Pathobiology and Mechanism of Disease. Biomolecules. 2021;11(1):75.
49. Sheikh TI, de Paz AM, Akhtar S, Ausió J, Vincent JB. MeCP2_E1 N-terminal modifications affect its degradation rate and are disrupted by the Ala2Val Rett mutation. Hum Mol Genet. 2017;26(21):4132-41.
50. Lee W, Kim J, Yun J-M, Ohn T, Gong Q. MeCP2 regulates gene expression through recognition of H3K27me3. Nature Communications. 2020;11(1).
51. Shahbazian MD, Antalffy B, Armstrong DL, Zoghbi HY. Insight into Rett syndrome: MeCP2 levels display tissue- and cell-specific differences and correlate with neuronal maturation. Hum Mol Genet. 2002;11(2):115-24.
52. Olson CO, Zachariah RM, Ezeonwuka CD, Liyanage VR, Rastegar M. Brain region-specific expression of MeCP2 isoforms correlates with DNA methylation within Mecp2 regulatory elements. PLoS One. 2014;9(3):e90645.
53. Moore LD, Le T, Fan G. DNA Methylation and Its Basic Function. Neuropsychopharmacology. 2013;38(1):23-38.
54. Li CH, Coffey EL, Dall'Agnese A, Hannett NM, Tang X, Henninger JE, et al. MeCP2 links heterochromatin condensates and neurodevelopmental disease. Nature. 2020;586(7829):440-4.
55. Li S, Peng Y, Panchenko AR. DNA methylation: Precise modulation of chromatin structure and dynamics. Curr Opin Struct Biol. 2022;75:102430.
56. Collins BE, Neul JL. Rett Syndrome and MECP2 Duplication Syndrome: Disorders of MeCP2 Dosage. Neuropsychiatric Disease and Treatment. 2022;Volume 18:2813-35.
57. Chahrour M, Jung SY, Shaw C, Zhou X, Wong STC, Qin J, et al. MeCP2, a Key Contributor to Neurological Disease, Activates and Represses Transcription. Science. 2008;320(5880):1224-9.
58. Leoh LS, van Heertum B, De Rijck J, Filippova M, Rios-Colon L, Basu A, et al. The stress oncoprotein LEDGF/p75 interacts with the methyl CpG binding protein MeCP2 and influences its transcriptional activity. Mol Cancer Res. 2012;10(3):378-91.
59. Jones PL, Veenstra GJC, Wade PA, Vermaak D, Kass SU, Landsberger N, et al. Methylated DNA and MeCP2 recruit histone deacetylase to repress transcription. Nature Genetics. 1998;19(2):187-91.
60. Bu Q, Wang A, Hamzah H, Waldman A, Jiang K, Dong Q, et al. CREB Signaling Is Involved in Rett Syndrome Pathogenesis. The Journal of Neuroscience. 2017;37(13):3671-85.
61. Coufal NG, Garcia-Perez JL, Peng GE, Yeo GW, Mu Y, Lovci MT, et al. L1 retrotransposition in human neural progenitor cells. Nature. 2009;460(7259):1127-31.
62. Yang J, Tian B, Brasier AR. Chapter One - Targeting Chromatin Remodeling in Inflammation and Fibrosis. In: Donev R, editor. Advances in Protein Chemistry and Structural Biology. 107: Academic Press; 2017. p. 1-36.
63. Blokken J, De Rijck J, Christ F, Debyser Z. Protein-protein and protein-chromatin interactions of LEDGF/p75 as novel drug targets. Drug Discov Today Technol. 2017;24:25-31.
64. Llano M, Morrison J, Poeschla EM. Virological and Cellular Roles of the Transcriptional Coactivator LEDGF/p75. Springer Berlin Heidelberg; 2009. p. 125-46.
65. Ortiz-Hernandez GL, Sanchez-Hernandez ES, Casiano CA. Twenty years of research on the DFS70/LEDGF autoantibody-autoantigen system: many lessons learned but still many questions. Autoimmunity Highlights. 2020;11(1).
66. Schrijvers R. The role of LEDGF/p75 in HIV replication [Doctoral thesis in biomedical science]. Leuven: KU Leuven; 2012.

67. Rozina A, Anisenko A, Kikhai T, Silkina M, Gottikh M. Complex Relationships between HIV-1 Integrase and Its Cellular Partners. International Journal of Molecular Sciences. 2022;23(20):12341.
68. Cermakova K, Weydert C, Christ F, De Rijck J, Debyser Z. Lessons Learned: HIV Points the Way Towards Precision Treatment of Mixed-Lineage Leukemia. Trends Pharmacol Sci. 2016;37(8):660-71.
69. Craigie R, Bushman FD. HIV DNA Integration. Cold Spring Harbor Perspectives in Medicine. 2012;2(7):a006890-a.
70. Janssens J, Bruggemans A, Christ F, Debyser Z. Towards a Functional Cure of HIV-1: Insight Into the Chromatin Landscape of the Provirus. Front Microbiol. 2021;12:636642.
71. Debyser Z, Vansant G, Bruggemans A, Janssens J, Christ F. Insight in HIV Integration Site Selection Provides a Block-and-Lock Strategy for a Functional Cure of HIV Infection. Viruses. 2018;11(1):12.
72. Pradeepa MM, Sutherland HG, Ule J, Grimes GR, Bickmore WA. Psip1/Ledgf p52 binds methylated histone H3K36 and splicing factors and contributes to the regulation of alternative splicing. PLoS Genet. 2012;8(5):e1002717.
73. Guy J, Hendrich B, Holmes M, Martin JE, Bird A. A mouse Mecp2-null mutation causes neurological symptoms that mimic Rett syndrome. Nature Genetics. 2001;27(3):322-6.
74. Nageshappa S, Carromeu C, Trujillo CA, Mesci P, Espuny-Camacho I, Pasciuto E, et al. Altered neuronal network and rescue in a human MECP2 duplication model. Molecular Psychiatry. 2016;21(2):178-88.
75. Sandweiss AJ, Brandt VL, Zoghbi HY. Advances in understanding of Rett syndrome and MECP2 duplication syndrome: prospects for future therapies. Lancet Neurol. 2020;19(8):689-98.
76. D'Mello SR. MECP2 and the biology of MECP2 duplication syndrome. Journal of Neurochemistry. 2021;159(1):29-60.
77. Herranz N, Gil J. Mechanisms and functions of cellular senescence. Journal of Clinical Investigation. 2018;128(4):1238-46.
78. De Cecco M, Ito T, Petrashen AP, Elias AE, Skvir NJ, Criscione SW, et al. L1 drives IFN in senescent cells and promotes age-associated inflammation. Nature. 2019;566(7742):73-8.
79. Thomas CA, Tejwani L, Trujillo CA, Negraes PD, Herai RH, Mesci P, et al. Modeling of TREX1-Dependent Autoimmune Disease using Human Stem Cells Highlights L1 Accumulation as a Source of Neuroinflammation. Cell Stem Cell. 2017;21(3):319-31.e8.
80. Stetson DB, Ko JS, Heidmann T, Medzhitov R. Trex1 Prevents Cell-Intrinsic Initiation of Autoimmunity. Cell. 2008;134(4):587-98.
81. Van Meter M, Kashyap M, Rezazadeh S, Geneva AJ, Morello TD, Seluanov A, et al. SIRT6 represses LINE1 retrotransposons by ribosylating KAP1 but this repression fails with stress and age. Nature Communications. 2014;5(1):5011.
82. Scheyltjens I, Laramée ME, Van den Haute C, Gijsbers R, Debyser Z, Baekelandt V, et al. Evaluation of the expression pattern of rAAV2/1, 2/5, 2/7, 2/8, and 2/9 serotypes with different promoters in the mouse visual cortex. J Comp Neurol. 2015;523(14):2019-42.
83. Van der Perren A, Toelen J, Carlon M, Van den Haute C, Coun F, Heeman B, et al. Efficient and stable transduction of dopaminergic neurons in rat substantia nigra by rAAV 2/1, 2/2, 2/5, 2/6.2, 2/7, 2/8 and 2/9. Gene Ther. 2011;18(5):517-27.
84. Bloh K, Kanchana R, Bialk P, Banas K, Zhang Z, Yoo BC, et al. Deconvolution of Complex DNA Repair (DECODR): Establishing a Novel Deconvolution Algorithm for Comprehensive Analysis of CRISPR-Edited Sanger Sequencing Data. Crispr j. 2021;4(1):120-31.
85. Mangeot PE, Risson V, Fusil F, Marnef A, Laurent E, Blin J, et al. Genome editing in primary cells and in vivo using viral-derived Nanoblades loaded with Cas9-sgRNA ribonucleoproteins. Nature Communications. 2019;10(1).
86. Kos CH. Cre/loxP system for generating tissue-specific knockout mouse models. Nutr Rev. 2004;62(6 Pt 1):243-6.
87. Rasband W, editor ImageJ, U.S. National Institutes of Health, Bethesda, Maryland, USA2011.

88. Bankhead P, Loughrey MB, Fernández JA, Dombrowski Y, McArt DG, Dunne PD, et al. QuPath: Open source software for digital pathology image analysis. Scientific Reports. 2017;7(1).
89. Bryant K. Guide to Understanding CRISPR Data Analysis Scores: Synthego; 2018 [2023-04-10]. Available from: https://www.synthego.com/blog/crispr-knockout-score#conclusion-know-your-knockout-score-when-analyzing-your-crispr-edits.
90. López-Otín C, Blasco MA, Partridge L, Serrano M, Kroemer G. The Hallmarks of Aging. Cell. 2013;153(6):1194-217.
91. Rahimi P, Mobarakeh VI, Kamalzare S, Sajadianfard F, Vahabpour R, Zabihollahi R. Comparison of transfection efficiency of polymer-based and lipid-based transfection reagents. Bratislava Medical Journal. 2018;119(11):701-5.
92. Liang X, Potter J, Kumar S, Zou Y, Quintanilla R, Sridharan M, et al. Rapid and highly efficient mammalian cell engineering via Cas9 protein transfection. J Biotechnol. 2015;208:44-53.
93. Lyu P, Wang L, Lu B. Virus-Like Particle Mediated CRISPR/Cas9 Delivery for Efficient and Safe Genome Editing. Life. 2020;10(12):366.
94. Royo NC, Vandenberghe LH, Ma J-Y, Hauspurg A, Yu L, Maronski M, et al. Specific AAV serotypes stably transduce primary hippocampal and cortical cultures with high efficiency and low toxicity. Brain Research. 2008;1190:15-22.
95. Zhang Y, Chen K, Sloan SA, Bennett ML, Scholze AR, O'Keeffe S, et al. An RNA-sequencing transcriptome and splicing database of glia, neurons, and vascular cells of the cerebral cortex. J Neurosci. 2014;34(36):11929-47.
96. Saunders A, Macosko EZ, Wysoker A, Goldman M, Krienen FM, De Rivera H, et al. Molecular Diversity and Specializations among the Cells of the Adult Mouse Brain. Cell. 2018;174(4):1015-30.e16.
97. Wither RG, Lang M, Zhang L, Eubanks JH. Regional MeCP2 expression levels in the female MeCP2-deficient mouse brain correlate with specific behavioral impairments. Exp Neurol. 2013;239:49-59.
98. Kalippke K, Werwitzke S, von Hornung M, Mischke R, Ganser A, Tiede A. DNA analysis from stool samples: a fast and reliable method avoiding invasive sampling methods in mouse models of bleeding disorders. Lab Anim. 2009;43(4):390-3.
99. Meldgaard M, Bollen PJ, Finsen B. Non-invasive method for sampling and extraction of mouse DNA for PCR. Lab Anim. 2004;38(4):413-7.
100. Parker MA, Anderson JK, Corliss DA, Abraria VE, Sidman RL, Park KI, et al. Expression profile of an operationally-defined neural stem cell clone. Exp Neurol. 2005;194(2):320-32.

LID VAN ASSOCIATIE KU LEUVEN